Joint CFR and DPD Optimization for 5G Digital Front Ends

Gustav Olsson

May 2023

Abstract

This thesis project investigates the topic of joint optimization for crest factor reduction and digital predistortion blocks, which are used for digital correction of analogue impairments in digital radio front ends. The work first investigates the effects of joint parameter variation of the above blocks on the global performance and computational cost of the digital chain, given reference CFR and DPD algorithms. Then it proposes a method for joint optimization of said CFR and DPD parameters, based on a constrained optimization of a composite target function. The constraints of this optimization problem ensure that the solution meets the requirements on out-of-band emissions and signal quality, while the target function values solutions that outperform these requirements and are computationally cheaper to implement. The solutions of such an optimization problem are determined with the help of simulations. The simulations provide estimated performance metrics on signal quality and out-of-band emissions as well as estimated computational cost for a given parameter configuration. The results show that the proposed optimization can guide the selection of parameters for multiple blocks of the DFE while ensuring applicability in different use-cases via an easily configurable target function.

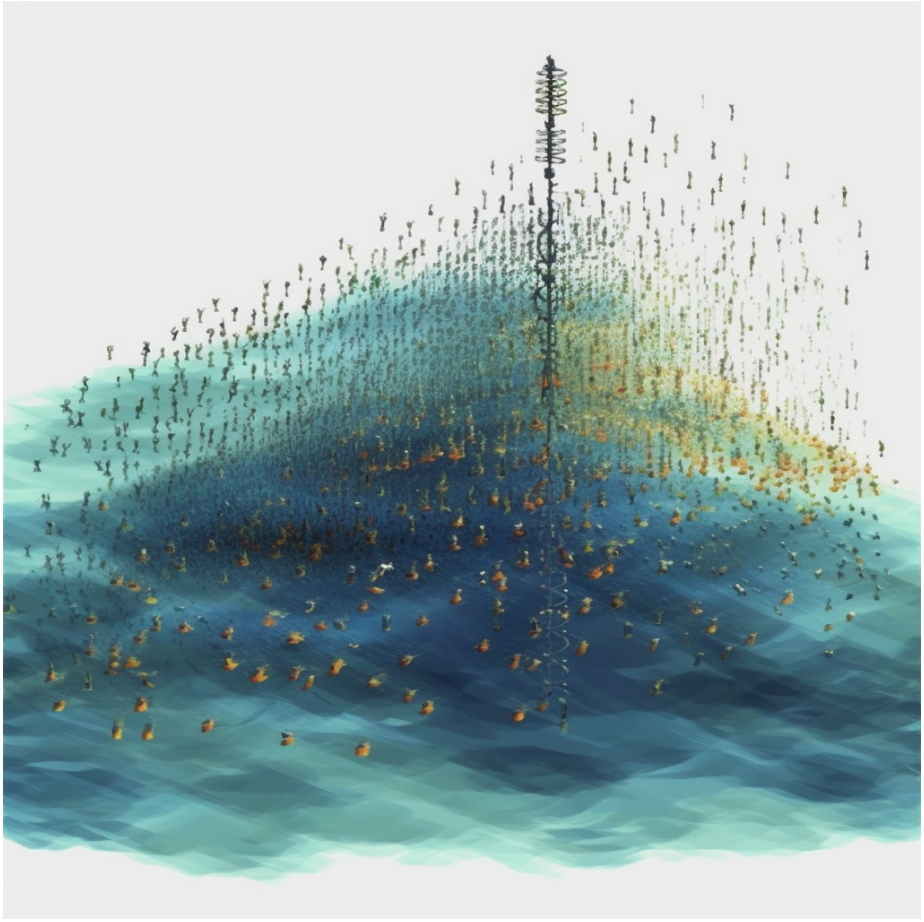

Acknowledgement

I would like to give a warm thank you to my main supervisor Simone Grimaldi who gave me more help, advice and support than I could possibly ask for throughout this thesis project. I would also like to thank my supervisor from the academic side, Tomas Persson. You helped me a lot with understanding the scope of a master thesis and the administrative road between its start and completion. Thank you, Hans Hagberg and Mohamed Hamid for taking the time to review my progress and give me monthly feedback. Thanks to all the members of the S&T RF technology team at Ericsson for the open and welcoming atmosphere in the office. I would like to thank Swedish taxpayer who helped finance my education. I would like to thank all my friends who helped me remember the importance of having fun and being social. Pappa, thank you for inspiring me to follow your footsteps and become an engineer. Mamma, thank you for always being there for me throughout my life.

Contents

List of Acronyms

5G 5^{th} Generation

ACEPR Adjacent Channel Error Power Ratio

ACL Adjacent Channel Leakage

ACLR Adjacent Channel Leakage Ratio

AMAM Amplitude to Amplitude

CFR Crest Factor Reduction

CR Clip Ratio

DFE Digital Front End

DPD Digital Predistortion

EM Electromagnetic

EVM Error Vector Magnitude

FIR Finite Impulse Response

FLOP Floating Point Operation

FLOPS Floating Point Operations per Second

FR Frequency Range

GMP Generalized Memory Polynomial

HL Hard Limiter

IQ In-phase Quadrature

MCFR Modelled Crest Factor Reduction

MP Memory Polynomial

NMSE Normalized Mean Squared Error

OBO Output Back-Off

OSR Oversampling Rate

PAPR Peak to Average Power Ratio

PEP Peak Envelope Power

PSD Power Spectral Density

QAM Quadrature Amplitude Modulation

RF Radio Frequency

List of Figures

List of Tables

Chapter 1

Introduction

The strength of a physical object is determined by how strongly its constituent parts are connected. By analogy one could say that the strength of a society is determined by the strength of the connections between its citizens. Wireless communication has revolutionized the speed at which information is shared and enables people to stay connected to their digital life and their loved ones from almost anywhere on earth.

This thesis will investigate how a small aspect within the realm of wireless communications can be improved.

There are countless types and use cases of wireless communication, but they are all based on the same basic principle. Information is embedded in electromagnetic (EM) waves by changing the properties of said wave, be it amplitude, phase or frequency, via a mechanism called modulation. This wave then travels through a medium from the sender to the receiver who picks up the signal through an antenna. The case being studied in this thesis is that of modern base stations used in mobile networks (e.g., in 5G networks).

In order for a radio-frequency (RF) signal to be transmitted with sufficient power, one or more RF amplification stages are needed. Amplifiers can behave as nonlinear systems with memory, which means that the behaviour of the system depends on the input signal level. Different power amplifiers (PA) have different amplification properties, but usually they behave linearly in the low-power region of the input signal and become more nonlinear for higher input power. To circumvent this, the power of the signal sent to the amplifier could be reduced so that no samples reach the nonlinear region. This works but is pretty wasteful since the amplifier is not operated at its optimal efficiency at low input power levels. If a signal has a high dynamic range, (contains both high and low power samples), different samples will get amplified with a different factor leading to increase out of band emissions and signal quality degradation. Both out of band emissions and signal quality are regulated by rigid requirements which need to be fulfilled by the radio system [2]. To sum up, there is a trade-off between efficient PA usage and output signal quality when the power of the input signal increases.
The Digital Front End (DFE) is the sub-system of the base station that performs a digital correction to the digital signals before they are converted to

analogue and sent to the analogue front end, which contains the PAs. The DFE is composed of several blocks. In the specific, the Digital Predistortion (DPD) and Crest Factor Reduction (CFR) blocks modify the input signal in order to operate the amplifier in the most efficient manner while minimizing the degradation of the transmitted signal. This thesis investigates an algorithm that jointly finds the optimal parameters for the CFR and DPD blocks with respect to the quality of the output signal and the computational cost of the implementation.

1.1 Thesis outline

This introductory chapter sheds light on the most central concepts of this thesis. Chapter 2 analyses some related literature on the subject and identifies research gaps on the topic of joint parameter optimization in digital front ends. This thesis proposes an investigation and an optimization method which aims to fill some of the identified gaps. Chapter 3 presents the proposed solution. Chapter 4 describes the methodology used to implement and test the proposed optimization algorithm through simulations. Chapter 5 presents the results from the simulations and their corresponding parameters in order to ensure reproducibility. The results will then be used to answer the research question in the conclusion chapter, which also highlights the limitations of the method and analysis in this thesis and provides directions for future works.

1.2 Power amplifiers

Power amplifiers can exhibit nonlinear behaviour which is not easy to predict and counteract. Furthermore, the nonlinear behaviour might include memory effects. Without the memory effect, any input value would be mapped to a single output value regardless of when it entered the PA or what inputs preceded it. With memory effects however, the same input could lead to different outputs depending on what values preceded it. The root cause of this lies in the electrical components of the amplifier.

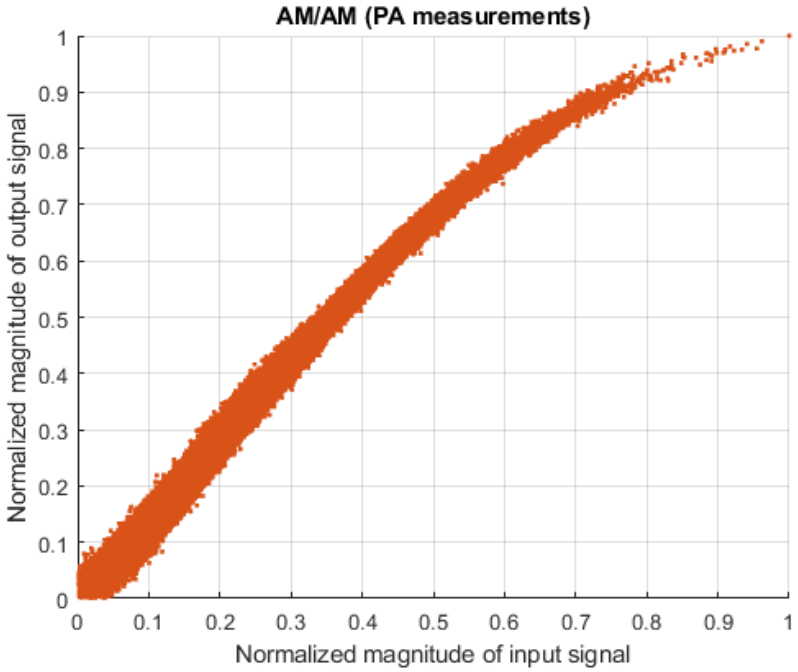

Figure 1.1: Example of a measured nonlinear input-output AM-AM response for an RF-PA.

Figure 1.1 shows the normalized amplitude of an unprocessed signal entering the PA vs the normalized amplitude of the signal at PA output. The first observation to be made is that there clearly is not a one to one relationship between input and output. Two samples with the same input magnitude can result in a range of different output magnitudes depending on the context they arrived to the PA. Secondly, the amplification decreases with increasing input power. This form of nonlinearity is called compression. This behaviour is clearly not acceptable since it will cause the quality of the transmitted signal to deteriorate and lead to out of band distortion. The goal is to be able to mimic the chaotic behaviour of the PA well enough that the distortions can be mitigated through digital predistortion of the input signal.

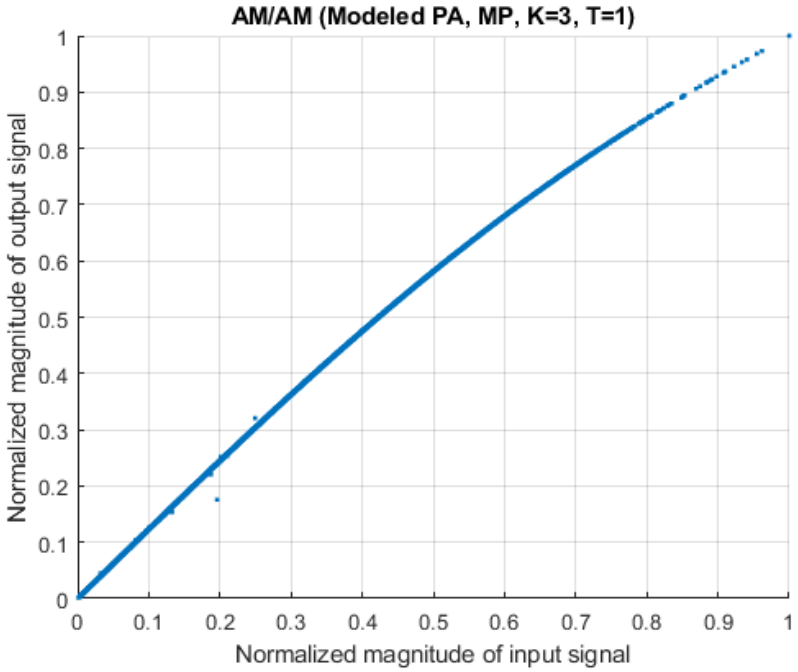

Figure 1.2: AM-AM response of a PA modelled with a third order memoryless polynomial model.

For example, assuming that the PA can be modelled with models based on memory polynomials (MP) (see Section 1.3), the non-linearities could be compensated for via estimating appropriate model parameters. Figure 1.2 shows how MP-model with nonlinearity order 3 and memory depth 1 (memoryless) would mimic the behaviour of the PA. The overall shape of the compression resembles the one in Figure 1.1, however the input-output relation is almost one to one, meaning that the model does not capture the memory effects at all.

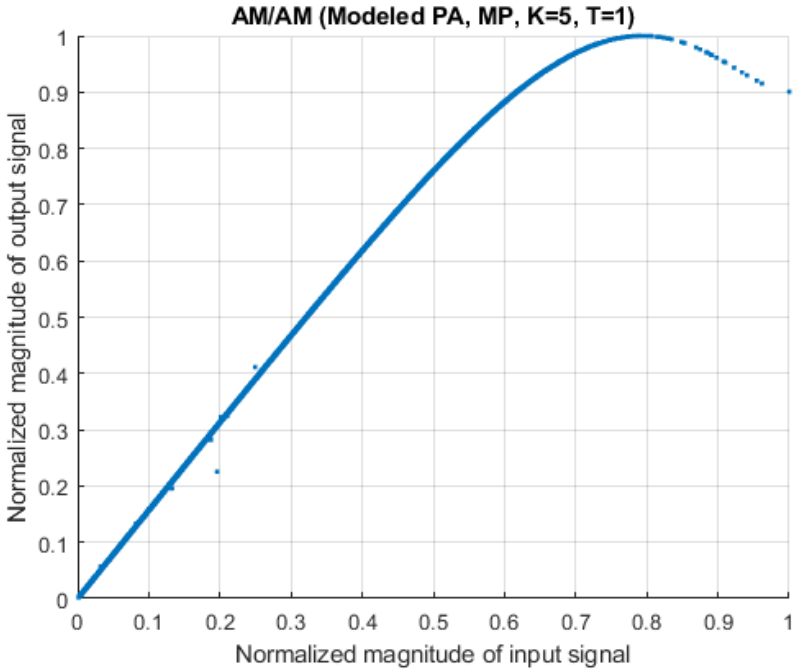

Figure 1.3: AM-AM response of a PA modelled with a fifth order memoryless polynomial model.

When the nonlinear order is increased from 3 to 5, as shown in Figure 1.3, the model recreates the nonlinearity slightly better than in Figure 1.2, however it is obvious that it still does not capture the memory effects due to lack of memory terms in the model.

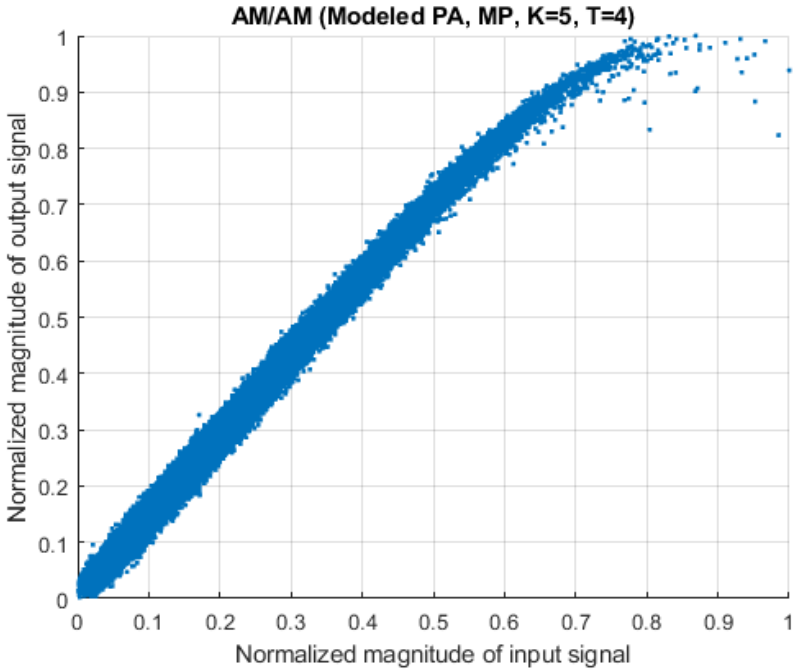

Figure 1.4: AM-AM response of a PA modelled with a fifth order memory polynomial model (6 memory taps).

In figure 1.4, the PA is modelled via an MP model with a nonlinear order of 5 and with a memory depth of 4. A comparison of Figures 1.1 and 1.4 gives a visual hint on the benefits of modelling PAs with richer nonlinear models, which is usually assessed by tracking the mean-squared error of the model.

1.3 Digital pre-distortion

A digital predistorter (DPD) is a digital processing block which compensates for the nonlinearity of the PA by applying a nonlinear distortion to its input signal. It can be shown that by selecting adequate nonlinear model and parameters for the DPD, the overall DPD+PA system behaves as quasi-linear. There are several DPD techniques and model available in the literature ([3] and references therein). Section 1.3.1 explains the memory polynomial model, which is part of the family of Volterra-based models, and it is used in this work.

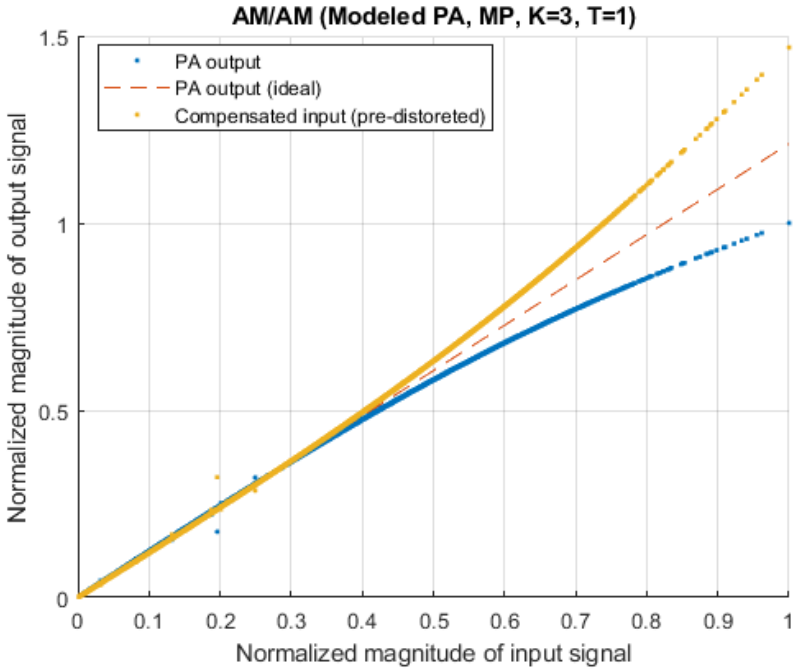

Figure 1.5: Example of AM-AM distortion for a memoryless PA and amplitude response of an ideal predistortion stage.

1.3.1 Memory polynomials

The most general way of modelling nonlinear systems with memory comes from the theory of Volterra series [4].

A system $x(t) \rightarrow \{h_n\} \rightarrow y(t)$, with $x(t)$ and $y(t)$ input and output signals, is defined by the Volterra series $\{h_n\}_{n\geq 1}$ if

$$y(t) = \sum_{n=1}^{\infty} \int_{\mathbb{R}^n} h_n(\tau_1, ..., \tau_n) x(t-\tau_1)...x(t-\tau_n) d\tau_1 ... d\tau_n$$

This sum of convolutions uses an infinite number of terms originating from past input values of the signal. This is not feasible in real applications, and we should also consider that the model is commonly implemented in digital blocks based on sampled signals (e.g., the DPD). A more practical model used in digital systems originates from a discretization the sum in the time domain. For example, we could choose to include in the sum a finite number (M) of previous samples, which are commonly called memory taps. The equation in discrete time then becomes:

$$y(n) = \sum_{k=1}^{K} y_k(n)$$

where

$$y_k(n) = \sum_{m_1=0}^{M-1} ... \sum_{m_k=0}^{M-1} h_k(m_1, ..., m_k) \prod_{l=1}^{k} x(n-m_l)$$

The above can be then used to derive a simplified expression for a memory polynomial (MP) model as [3]

$$y_{MP}(n) = \sum_{k=0}^{K-1} \sum_{m=0}^{M-1} a_{km} x(n-m)|x(n-m)|^k \tag{1.1}$$

The (1.1) can be then further extended to the generalized memory polynomials (GMP) model [3] by including cross-memory terms as

$$\begin{aligned} y_{GMP}(n) &= \sum_{k \in K_a} \sum_{l \in L_a} a_{kl} x(n-l)|x(n-l)|^k \\ &+ \sum_{k \in K_b} \sum_{l \in L_b} \sum_{m \in M_b} b_{klm} x(n-l)|x(n-l-m)|^k \\ &+ \sum_{k \in K_c} \sum_{l \in L_c} \sum_{m \in M_c} c_{klm} x(n-l)|x(n-l+m)|^k \end{aligned}$$

1.4 Crest factor reduction

As described in Section 1.2, signals with very wide dynamic range are undesirable as they cause higher peaks in the compression region of the PA for the same average input power, with respect to signals with lower dynamic range. This is generally quantified by the peak-to-average power ratio of a signal, which we describe in Section 1.6. To counteract this, the PAPR of input signals is reduced using Crest Factor Reduction techniques (CFR).

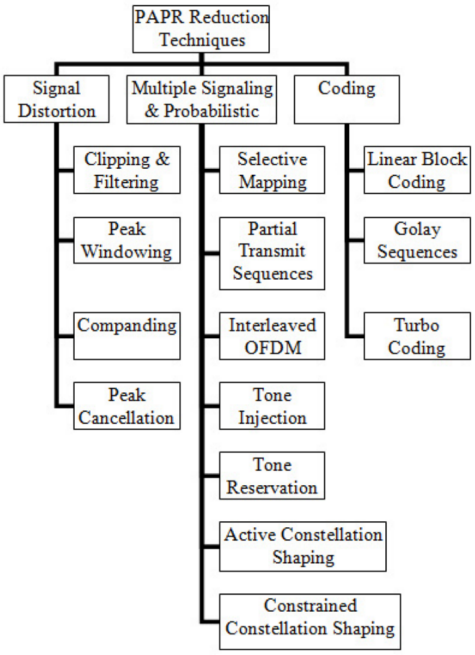

Figure 1.6: Taxonomy of CFR techniques [1]

Figure 1.6 is taken from [1] and shows several families of PAPR reduction techniques categorized into three main groups:

- Signal distortion
- Multiple signalling and probabilistic
- Coding based

While we remind to reference literature for an overview of these techniques, this investigation assumes a clip-and-filter CFR technique, which falls within the signal distortion category.

1.4.1 Clip and Filter

The crest factor reduction technique studied in this thesis is Clip and Filter (CF). This method involves several steps which are sketched in Figure 1.7 below.

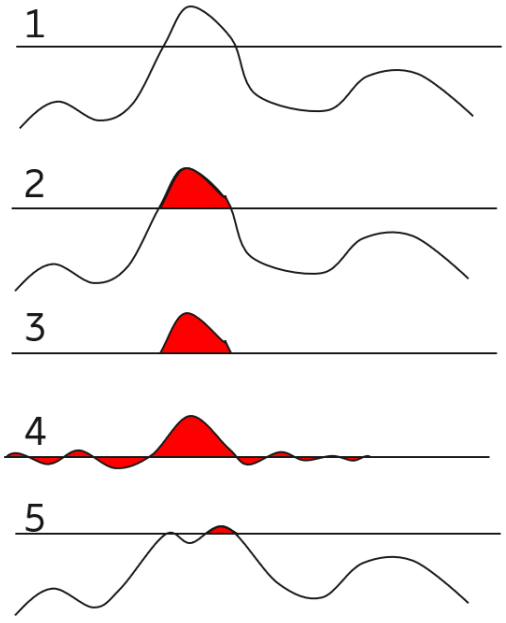

Figure 1.7: The steps of the Clip-and-Filter algorithm.

First, a threshold is set which dictates which samples of the signal will be clipped. In the second step, the samples exceeding the threshold are identified, then they are extracted in the third step. This extracted signal is then filtered in the fourth step and finally subtracted from the original signal in the fifth step.

The output signal will then present reduced peak power compared to the input signal, while some samples will still be above the threshold due to the filtering process. This phenomenon is commonly called peak regrowth.

A possible solution to handle the peak regrowth is to cascade multiple clip-and-filter blocks. The approach is represented in Figure 1.8 and will be used later in this thesis as the reference CFR technique.

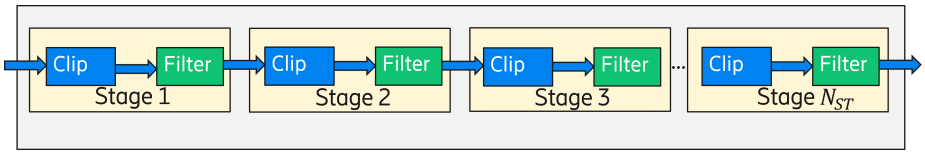

Figure 1.8: Block diagram of multi-stage clip-and-filter CFR

Figure 1.9 illustrates how the dynamic range of a signal has been reduced after CFR, compared to the distribution of the input signal that we show in Figure 1.11. The CFR output signal presents fewer high-energy samples (leading to a lower PAPR) allowing the PA to operate at a higher, more efficient level.

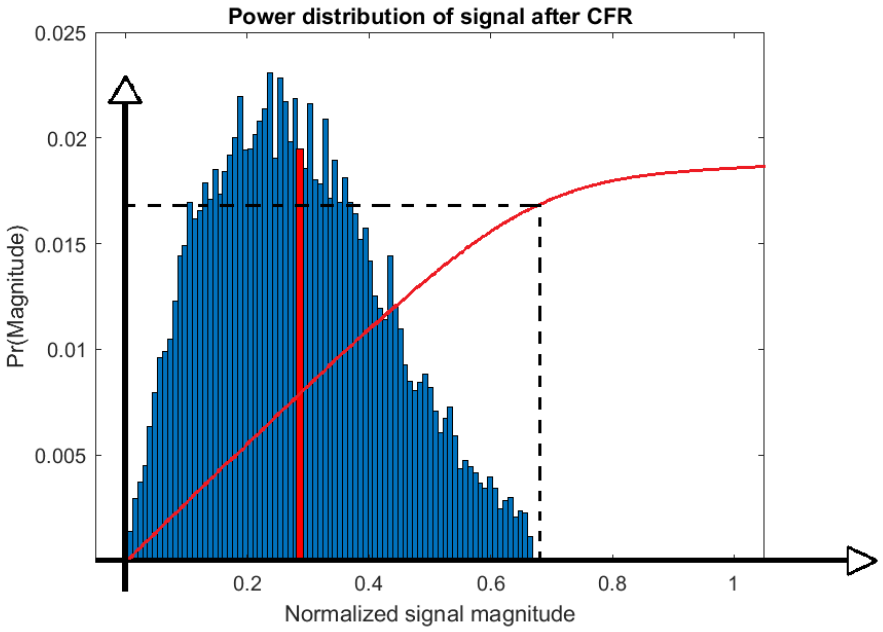

Figure 1.9: Distribution of signal amplitude after CFR vs. PA input-output response.

1.5 Signal parameters and performance metrics

The RF signals radiated by the base station are subject to strict requirements on both signal quality (i.e. the accuracy of the transmitted time domain waveform with respect to the wanted one) and out of band emissions. Furthermore, also the input signal to RF PA needs to be controlled with respect to certain parameters e.g. the peak envelope power(PEP) in order to operate the unit within specifications.

1.5.1 ACLR

The adjacent channel leakage/power ratio (ACLR)/(ACPR) quantifies the ratio of signal power transmitted in an adjacent channel with respect to the signal power transmitted in the wanted channel. That is,

$$\text{ACLR} = \frac{P_{adj}}{P_{ch}}$$

where P_{ch} is the power radiated in the assigned channel and P_{adj} is the total power leaked into the adjacent channel. If the channel in question has two adjacent channels, then the channel experiencing the highest out of band leakage is used to calculate ACLR.

ACLR is usually indicated in logarithmic units (dBc, dB-carrier). The 3GPP standard [2] sets stringent requirements on the ACLR, e.g., < -45 dBc for frequency-range 1 (FR1).

The ACLR can be negatively affected both by PA nonlinearity (i.e., spectral expansion) and from aggressive signal processing (e.g, hard-clipping the signal).

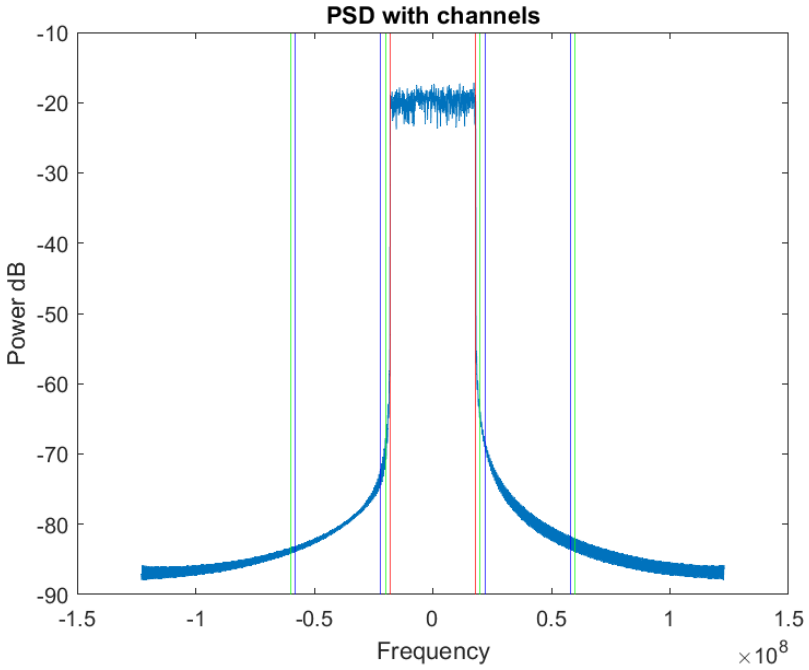

Figure 1.10: PSD over the main channel and the adjacent channels.

Figure 1.10 shows the center-shifted power spectral density (PSD) of a signal overlaid with vertical bars. The red and blue bars shows the location of the main channel and the adjacent channels respectively. The green bars show the limits between the bands. The guard bands are represented by the distance between the red and green bars for the main channel and the distance between the blue and green bands for the adjacent channels.

1.5.2 Peak-to-average power ratio

Peak-to-average power ratio (PAPR) is a metric quantifying the crest factor of a signal. It carries information on the relation between the maximum peak power of the signal and its average value.

$$\mathrm{PAPR}(x[n]) = \frac{\max(x[n])^2}{E(|x[n]|^2)} \tag{1.2}$$

where $\max(x[n])^2$ represents the maximum IQ sample power and $E(|x[n]|^2)$ represents the average power of the signal.

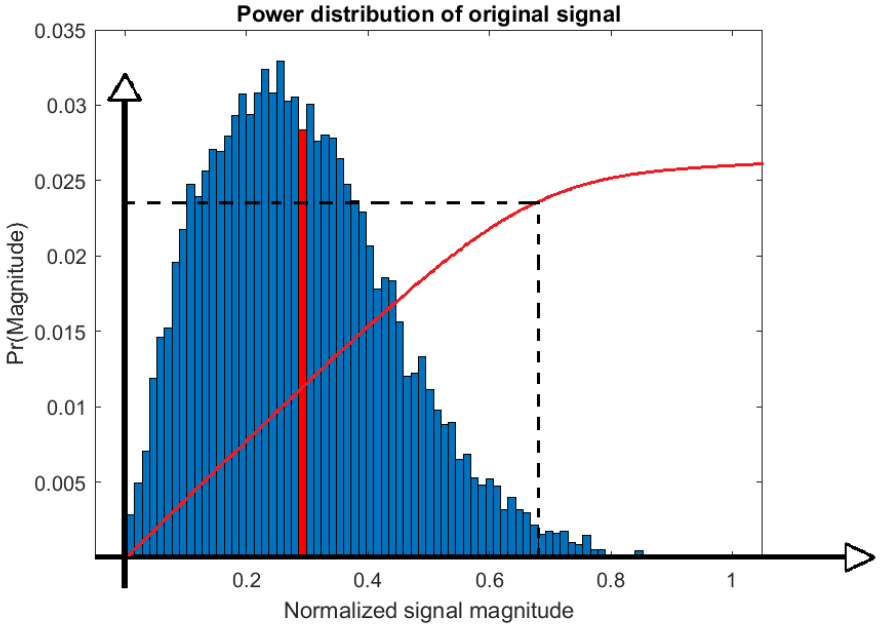

Figure 1.11: Power distribution overlaid on PA's linearity

Figure 1.11 provides an example of the empirical distribution of the magnitude of a complex signal. We can observe that most samples fall within the $0\% - 60\%$ region of the largest sample and almost none fall in the top 20%. In practice those few peaks will result in a high PAPR, which is undesirable in order to operate the PA efficiently. This is because a high PAPR will result in high peak-envelope power (PEP), which is defined as the RMS power (in dBm) in plus the PAPR (in dB). Since RF-PA can tolerate up to a maximum PEP for the input signal, a high PAPR will force to reduce the input power (power back-off) which is undesirable as it reduces PA efficiency.

1.5.3 Error vector magnitude

Electromagnetic waves can encode data in several different ways. In this case binary data is transmitted by modulating the signals phase and amplitude in

the IQ-plane. A signal can represent different bits depending on where its vector points in the IQ-plane. An example of this is Quadrature Amplitude Modulation or QAM. QAM comes in different versions depending on how many points the IQ-vector can point to. For example, if the constellation is composed by 16 symbols, the modulation is named 16 QAM. Figure 1.12 illustrates these points and the data they represent.

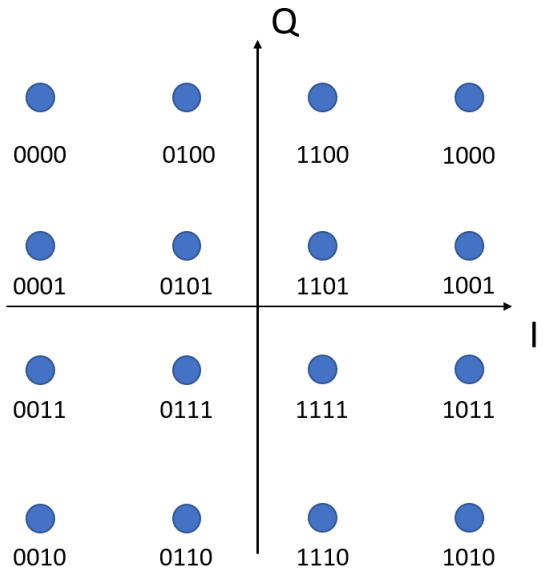

Figure 1.12: Illustration of 16 QAM constellation.

Distortions and noise that act on the transmitted signal can cause the vector to point to a different area than intended. The difference between these two vectors is called the compared to the distribution of the input signal that we show in Figure 1.13. The metric commonly used to compare this type of deviation is called Error Vector Magnitude (EVM) and simply refers to the length of the error vector. The EVM is often expressed as a percentage of the length of the ideal, error-free vector.

$$EVM\% = \frac{\sqrt{\frac{1}{N}\sum_{n=0}^{N-1} I_{err}[n]^2 + Q_{err}[n]^2}}{R_{nor}}$$

Where n is the signal sample index, N is the total number of samples in the signal, I_{err} is the in-phase error between the reference vector and the actual vector, Q_{err} is the quadrature error between the reference vector and the actual vector, and R_{nor} is a reference normalization value (e.g., the RMS level of the signal).

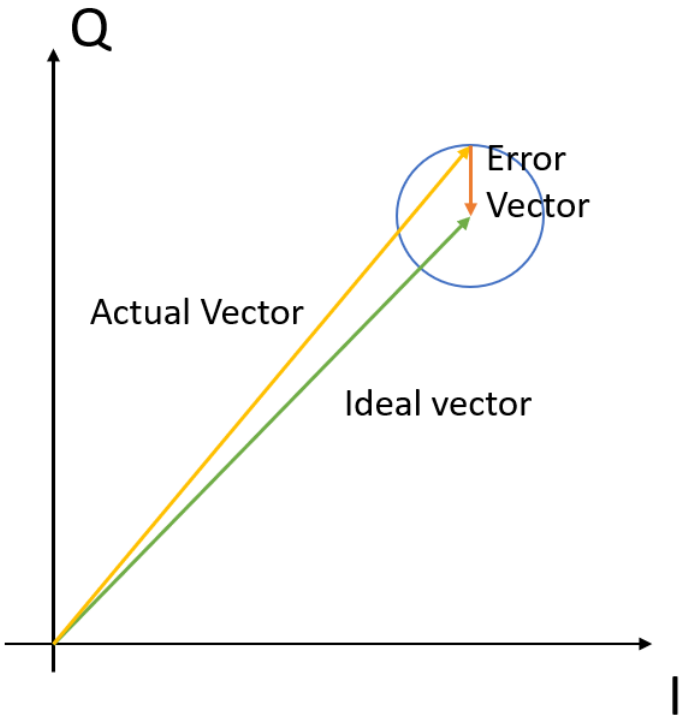

Figure 1.13: Error vector in the IQ-plane.

Chapter 2

Literature Review

Throughout this investigation, knowledge has been continuously drawn from different sources, mainly articles. This section showcases some of the research that has been done around the topic of this thesis. The aim is to identify what has been done, but more importantly, what has not been done. This thesis aims to address some of the gaps that have been identified and described in this section.

2.1 DPD

The article "A Comparative Analysis of the Complexity/Accuracy Trade-off in Power Amplifier Behavioural Models" [5] studies the computational cost of implementing different predistortion techniques on two different power amplifiers. This computational cost is expressed in terms of FLOPS and weighted against the error metrics normalized mean squared error (NMSE) and adjacent channel error power ratio (ACEPR). All the models tested were parameter based, and the models perform differently depending on how many parameters they were allowed to have. This study also took the maximum number of parameters into account and let this number vary from 1 to 1000. It was found that the generalized memory polynomial model (GMP) had the best complexity/accuracy trade-off for both amplifiers. However, the MP model resulted in the lowest error when only few parameters were used. An interesting idea in this paper was to plot computational cost vs. accuracy for each parameter configuration and constructing the convex hull [6]. This hull then contains all the best configurations with respect to the complexity/accuracy trade-off.

2.2 CFR

"A Novel Crest Factor Reduction Technique using Memoryless Polynomials" [7] discusses many topics that tie into this thesis. It compares the effects that different CFR techniques have on ACLR and EVM, while phenomenon such as peak regrowth and spurious emission are studied, and an optimization problem is set up. In this case the PAPR is reduced by distorting the signal using memoryless polynomials. The convex optimization problem aims to minimize the PAPR by adjusting the polynomial coefficients of the distortion signal. The

problem is subject to constraints in EVM and ACLR in that they both must be lower than a certain limit.

2.3 Combined CFR and DPD

"Impacts of Crest Factor Reduction and Digital Predistortion on Linearity and Power Efficiency of Power Amplifiers" [8] is probably the article with the closest area of investigation compared to that of this thesis. This article considers a joint CFR and DPD optimization with respect to computational cost. The main investigation begins on how different positions of the CFR block in relation to the DPD block affect the computational cost (and consequently the power consumption of the digital part). A merit function is introduced that evaluates the ability of CFR to improve the PA's power efficiency. This function has a weight coefficient included in the computational cost in relation to the output back-off. The results showed that their joint Modelled Crest Factor Reduction (MCFR) technique produced improvements compared to concurrent solutions in the literature in terms of trade-off among linearity, PA power efficiency and CFR complexity.

2.4 Research Gaps

The solution in [5] does not use CFR to mitigate some of the issues caused by the power amplifier, instead it uses the power back off technique. This is a lost opportunity since it means that the PA is operated at a suboptimal level leading to lower signal range and worse power efficiency.

While [7] formulates a detailed optimization algorithm for the memoryless polynomial technique, used to perform CFR, it does not cover the clip-and-filter strategy. The algorithm does not factor in computational complexity which is also something that could be included in the cost function to be minimized.

The authors of article [8] investigate the effects of putting the CFR block before or after the DPD, in terms of CFR computational complexity and output back-off (OBO) (how much the signal needs to be backed off before going through the PA). While the technique obviously contains a DPD block, the DPD model itself is not considered as part of the investigation. The merit function only takes into account the OBO and computational complexity. More performance metrics could be taken into account.

2.5 Proposed investigation

The current thesis proposes an investigation into joint CFR and DPD parameter optimization. An algorithm selects the feasible solutions from this parameter space given constraints and selects the optimal solution with the help of a composite and user-tunable cost function. Such a function includes information on signal quality, out-of-band emissions, and computational cost of the entire DFE chain.

Differently from the related literature this thesis investigates a method for joint optimization of CFR and DPD blocks which is not bounded by the specific models used in the blocks. Furthermore, the extension of the optimization to other

blocks of the digital front end (DFE) is also investigated. Chapter 3 explains the details of the proposed solution.

Chapter 3

Proposed Solution

The problem at hand in a nutshell is: signals passing through the amplifier get deteriorated because of its nonlinearity and memory effects. There are regulations that impose requirements on the ACLR and EVM of the transmitted signal [2]. The CFR block mitigates this by reducing the signals PAPR before it enters the DPD block. The DPD block uses a model of the amplifier to distort the signal in such a way as to compensate for its imperfections.

The problem is to calibrate the CFR and DPD parameters in a way that minimizes the EVM and ACLR of the transmitted signal as well as the computational cost of running the blocks.

3.1 Overview of the proposed solution

There are many parameters that can be tuned in a CFR block, and they depend on the specific algorithm and implementation. For this investigation we have chosen to restrict the analysis to some of the most essential parameters of a clip-and-filter CFR, that are, clip ratio and filter length. The DPD can also have multiple parameters to calibrate (memory tap selection, internal oversampling) but we select only two fundamental parameters for the investigation. Those are the maximum nonlinearity order, and the number of memory taps in the reference MP model.

Since the input-output relation of the PA is too complex to be expressed algebraically it is difficult to express ACLR and EVM in terms of the CFR and DPD variables. A simulation-based approach is therefore used instead. All four variables are varied at once creating one 4D parameter space for each of the monitored performance metrics (ACLR, EVM, PAPR) These results will then be used in the following optimization problem

$$\underset{\mathbf{p}}{\text{minimize}} \quad f(C(\mathbf{p}), EVM(\mathbf{p}), ACLR(\mathbf{p}))$$

$$\text{Subject to} \begin{cases} EVM(\mathbf{p}) \leq EVM_{lim} \\ ACLR(\mathbf{p}) \leq ACLR_{lim} \\ PEP(\mathbf{p}) \leq PEP_{high} \\ P_{low} \leq P_{RMS} \leq P_{high} \end{cases}$$

where $\mathbf{p} = [\mathbf{p}_D \quad \mathbf{p}_C] = [K_{DPD}, M_{DPD}, \theta_{CFR}, L_{CFR}, \dots]$ is a vector of parameters including different parameters of blocks in the Digital Front End (DFE) chain, and with $f(C(\mathbf{p}), EVM(\mathbf{p}), ACLR(\mathbf{p}))$ being the objective function including an arbitrary combination of the total computational cost $C(\mathbf{p})$ and the performance metrics (EVM and ACLR). The employed formulation of the objective function will be detailed in the next sections.

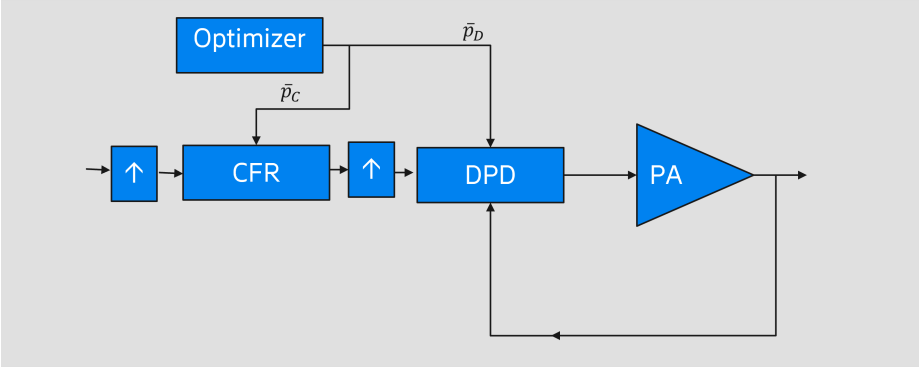

Figure 3.1: Illustration of the optimizer operating on a DFE chain with DPD, CFR and related up-sampling blocks.

Figure 3.1 illustrates the role of the optimizer in relation to the DFE chain, where the blocks containing an upward arrow symbolize up-sampling.

When exploring the parameter space, we might find that several sets of input parameters generate feasible solutions, i.e., solutions which satisfy arbitrary requirements on performance metrics and/or complexity. The question is then: How do we compare and rank the feasible solutions? When performing optimization, we need a target function to minimize. In this case we want to prioritize solutions that use fewer floating point operations per second (FLOPS) and solutions that give wider margin between their EVM, ACLR and their corresponding limits.

3.2 Objective function

The aim the proposed objective function is to reward solutions that are computationally cheap while leaving a larger margin between the achieved EVM/ACLR and the worst acceptable EVM/ACLR (the constraints). The objective function will therefore depend on more variables than just the total number of FLOPS, that is

$$C_{tot}^{FLOPS} = C_{CFR}^{FLOPS} + C_{DPD}^{FLOPS}$$

The proposed cost function below reflects these characteristics

$$f(C, EVM, ACLR) = a\frac{C_{tot}^{FLOPS}}{C'_{max}} + b\frac{EVM}{EVM_{const}} + c\frac{ACLR}{ACLR_{const}}$$

were C'_{max} is the maximum tolerable computational cost, while the factors a, b, c assign weights depending on how important the corresponding term is. The

higher the factor, the more important it is for the corresponding metric to be minimized.

Let us consider two different cost functions where $a = 1, \quad b = 1, \quad c = 1$ and $a = 1, \quad b = 2, \quad c = 1$ to illustrate the effects of the weight factor b. Let us also consider the set of solutions where ACLR and computational cost are the same and the EVM is allowed to vary. If there are two solutions in this set, where $2EVM_{sol1} = EVM_{sol2}$, then plugging in EVM_{sol1} in the first objective function where $a = 1, \quad b = 1, \quad c = 1$ and EVM_{sol2} in the second where $a = 1, \quad b = 2, \quad c = 1$ would generate the same objective value. That means that the second objective function increases the weight of EVM in the objective and therefore favours solutions with lower EVM. The same reasoning can be applied to increase the weight of ACLR, computational cost, or a combination of these.

3.3 Estimation of computational costs

3.3.1 Estimation of computational cost for the DPD block

This part of the cost function is based on the findings in [5]. The number of floating point operations per sample is calculated in two parts, the first corresponds to when the basis functions are generated $C_{basis}(K, M) = 3(K + 1)$, where K is the nonlinear order and M is the number of memory taps, and the second part corresponds to the filtering, that is

$$C_{filter}(K, M) = 8 \cdot \frac{K + 1}{2} \cdot (M + 1) - 2$$

The total estimated FLOPs per sample is $C_{DPD}(K, M) = C_{basis}(K, M) + C_{filter}(K, M)$, which can therefore be rewritten as

$$C_{DPD}(K, M) = 3(K + 1) + 8 \cdot \frac{K + 1}{2} \cdot (M + 1) - 2$$

$$= 4(K + 1)(M + 1) + 3K + 1$$

We now take into account the specific sample-rate of the DPD and express the estimated computational cost for the DPD in terms of floating points operations per second (FLOPS), that is

$$C_{DPD}^{FLOPS}(\mathbf{p}_D) = R_{DPD} C_{DPD}(\mathbf{p}_D)$$

where R_{DPD} is the sample rate of the DPD block, which is usually higher than the CFR sample rate. There are two reasons for this: to allow linearizing desired adjacent channels, and to accommodate wider spectrum for DPD basis functions. Since R_{DPD} is a function of the maximum nonlinearity order, we could rewrite the DPD cost as

$$C_{DPD}^{FLOPS} = R_{DPD}(K) C_{DPD} = \left[L \frac{B_S}{R_s} \right] C_{DPD}$$

where B_S is the bandwidth and R_S the IQ-rate of the digital baseband signal.

An observation to the above relation is that it assumes that we are able to oversample the signal to operate exactly at required DPD rate $R_{DPD}(K)$. In practice this might change due to integer up-sampling operated at different stages in the DFE.

3.3.2 Estimation of computational cost for the CFR block.

The computational cost for a generic clip-and-filter CFR can be taken from [8]

$$C_{CFR,PF}(\mathbf{p}_C) = \sum_{n=1}^{N_{ST}} 14 + N_p(n)(6 + N_{FIR})$$

where $N_{FIR} = 6W + 2(W - 1)$ is the number of FLOPS used by a FIR filter of length W, and $N_p(n)$ number of clipped peaks at each of the N_{ST} CFR stages. In terms of FLOPS it becomes:

$$C^{FLOPS}_{CFR,PF}(\mathbf{p}_C) = R_{CFR} C_{CFR,PF}(\mathbf{p}_C)$$

where R_{CFR} is the sample rate of the CFR block.

Let us now consider a multi-stage CFR algorithm. For single branch CFR, the computational cost in terms of FLOP does not depend on the number of clipped peaks N_p, and can be approximated as:

$$C_{CFR,MC}(\mathbf{p}_c) = N_{ST} R_{CFR}(N_{CLIP} + N_{AD} + N_{FIR}(\mathbf{p}_c))$$

Where N_{ST} is the number of clip-and-filter stages, N_{CLIP} is the FLOPs of the hard-clipper stage, N_{AD} the FLOPs needed for the sample-rate adaptation, and $N_{FIR}(\mathbf{p}_c)$ the FLOPs needed for each peak-filtering stage.

Chapter 4

Methodology

The strategy used to test the proposed approach is based on simulations. The DFE blocks of interest (CFR, DPD, up-sampler and hard limiters) have been implemented in a MATLAB-based simulator. An MP-based PA model has been used to simulate the behaviour of real RF-PA. This chapter provides more details on the implementation of the aforementioned blocks.

4.1 Simulation and code setup

The programming language used to develop the simulator employed in this thesis is MATLAB. The simulator implements three main blocks, which are: the CFR and DPD as part of the simulated DFE, and a modelled PA.

4.1.1 CFR

The CFR part implements a custom clip-and-filter-based algorithm where parameters such as clipping threshold, number of clip-and-filter stages, etc can be tuned. The CFR block is preceded by an upsampling stage which adapts the sample rate of the input signal to a rate suitable for the CFR. The up-sampler is set to provide an oversampling factor of 3 in order to accommodate for the distortion at the CFR level. Then error metrics and PAPR were computed and plotted using separate functions.

4.1.2 DPD

The DPD part is the most central part of the code since it receives input from the CFR section and applies a memory polynomial model to predistort the signal in relation to the PA's behaviour. Several structs are used to store general parameters and DPD model parameters respectively.

The algorithm used to estimate DPD coefficients estimation works as follows. The signal is run through the modelled PA and the output is used to estimate the PA gain and the ideal output. This is then used to generate an ideal predistortion using the iterative learning control (ILC) technique [9] illustrated in Figure 4.1. The DPD-model coefficients for this ideal predistorted signal are then estimated via least squares estimation [3] and the target input is then fed through the adapted DPD-model. Finally, the predistorted signal passes

through the PA. The output of the PA with respect to the predistorted input is measured and relevant metrics (EVM, ACLR) are calculated and stored.

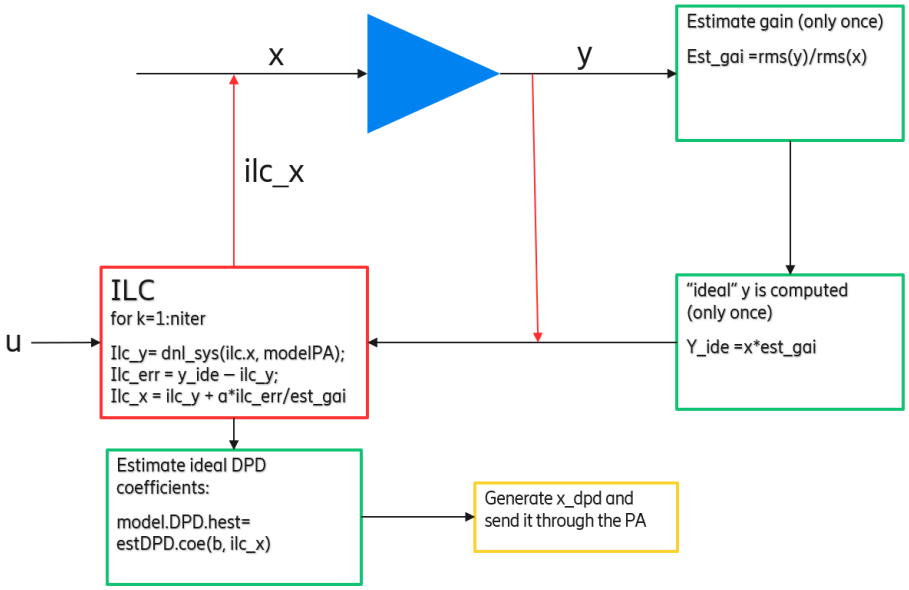

Figure 4.1: Block diagram of the adaptation phase of the DPD block via ILC algorithm.

4.1.3 PA

The employed PA model is based on a memory polynomial approach, which has been trained on data measured on a real Doherty-PA [10]. The maximum non-linearity order used in the MP model is 9 while the number of lagging memory taps is 6.

4.1.4 Metrics

To begin with, functions to calculate the metrics PAPR, EVM, NMSE and ACLR, detailed in Chapter 1, were implemented as well as visualization routines to monitor the metrics during simulation runs.

Chapter 5

Results and Discussion

This section covers the results of two main investigations. First, the effects of joint variation of CFR and DPD parameters on performance metrics and computational complexity of the DFE are investigated in Sections 5.1, 5.2, and 5.3. The investigation is then expanded to the case where a hard-limiter block is introduced between the CFR and the DPD, which is covered in Section 5.4.

Second, the constrained optimization approach described in Section 3 is used to optimize an exemplary subset of parameters of the above DFE chains (with and without hard-limiter block). The results of this optimization are discussed in Section 5.5. In that section we also show different configurations of the proposed objective function and their impact on the outcome of the optimization.

5.1 The effect of varying CFR parameters

In this section of the investigation the parameters in the DPD block are kept constant while we vary the clipping ratio and number of taps of the FIR filter used in the clip-and-filter CFR block. Table 5.1 below shows the value of the variables that are kept constant throughout all the simulations in Sections 5.1, 5.2 and 5.3.

Signal bandwidth	40MHz
CFR: Oversampling ratio	3
CFR: Number of stages	4
DPD: Oversampling ratio	Varies with NLO
Number of ILC iterations	5
PA model: Type	MP
PA model: Maximum nonlinear order	9
PA model: Number of memory taps	6

Table 5.1: Global simulation parameters (constant).

5.1.1 Varying CFR clip ratio and filter length

DPD maximum nonlinear order	DPD number of memory taps
9	5

Table 5.2: Constant parameters: clip ratio vs. filter length

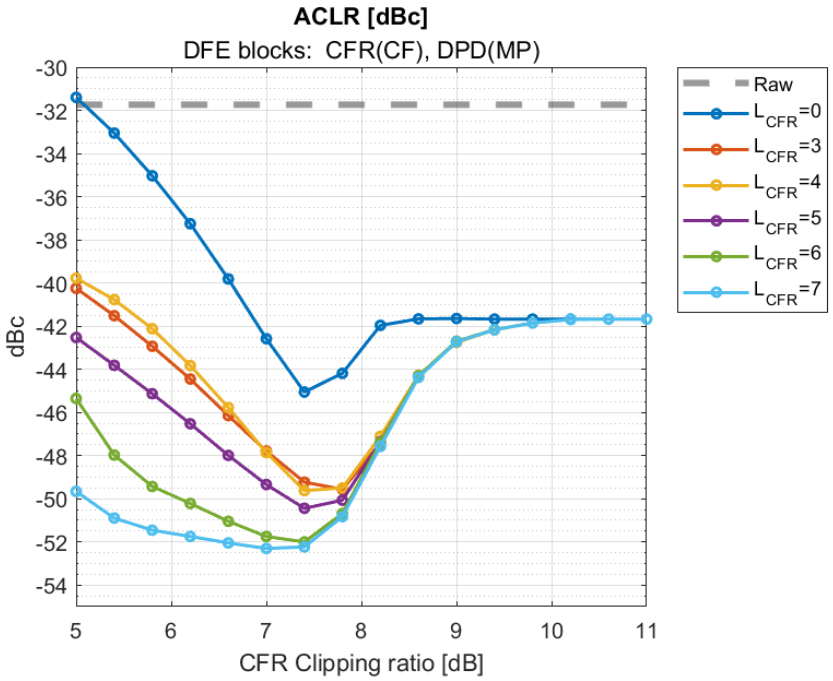

Figure 5.1: ACLR at PA output as a function of CFR clip ratio and filter length (L_{CFR})

Figure 5.1 shows that the lower the clipping ratio, the lower the threshold which means more peaks are clipped. Starting at a clip ratio of over 10 dB no peaks are clipped therefore there is no signal to be filtered. If there is nothing to be filtered, then the filter length has no impact on the ACLR and all the curves corresponding to different filter lengths overlap in this region. As the clip ratio is decreased more and more of the signal is clipped therefore there are more clipped peaks causing ACLR degradation. Filtering mitigates this, and the longer the filter the better it "smoothes out" the leakage caused by the clipping. This is why the overlaping curves diverge. The ones with higher filter lengths result in better ACLR and vice versa, The only exception being $L_{CFR} = 0$ which corresponds to no filtering (hard clipping) in the CFR.

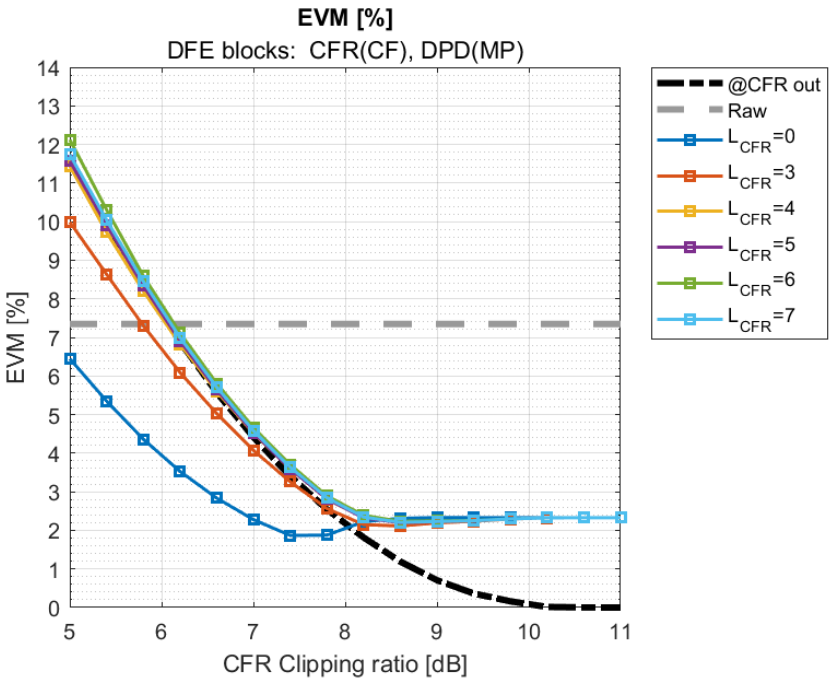

Figure 5.2: EVM at PA output as a function of CFR clip ratio and filter length (L_{CFR})

In Figure 5.2 we see that, similarly to the ACLR analysis, the curves of the different filter lengths overlap when we do not clip the input signal. As the threshold is lowered, the curves separate and the shorter filters result in better EVM. The best EVM is obtained when the signal is not filtered at all which makes sense since no filter means that the clipped signal remains unchanged until it arrives at the DPD block. Filters with lengths 4-7 are clustered together while the one of length 3 seems to perform slightly better.

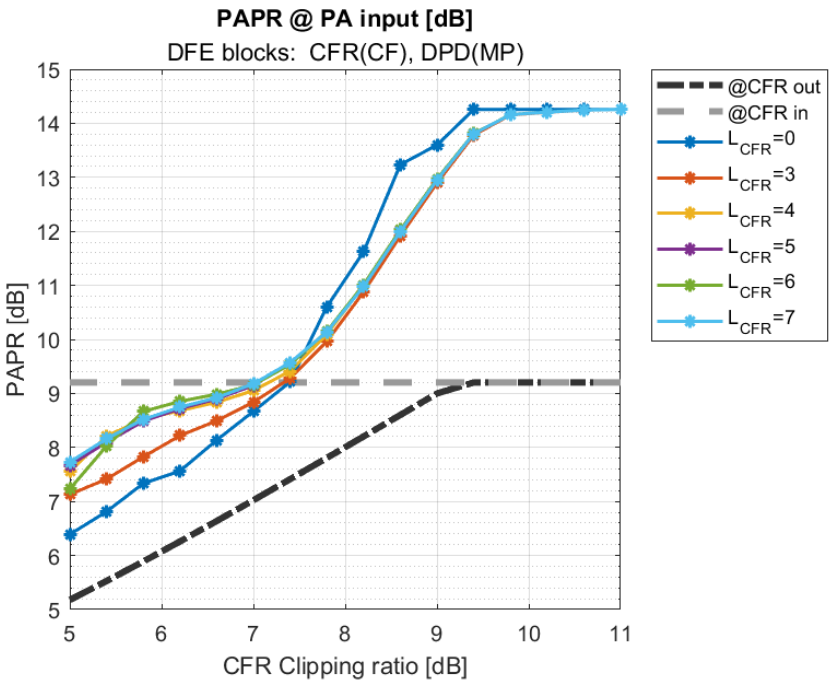

Figure 5.3: PAPR at PA input as a function of CFR clip ratio and filter length (L_{CFR})

Figure 5.3 shows the PAPR of the input signal to the PA, while we take care of keeping the RMS of the output signal constant (variations within a ± 0.1 dB range). As expected, lowering the clip ratio results in an input signal with lower PAPR. Furthermore, using longer FIR filters leads to a more pronounced phenomenon of peak regrowth, leading to higher PAPR at the advantage of better ACLR suppression (see Figure 5.1).

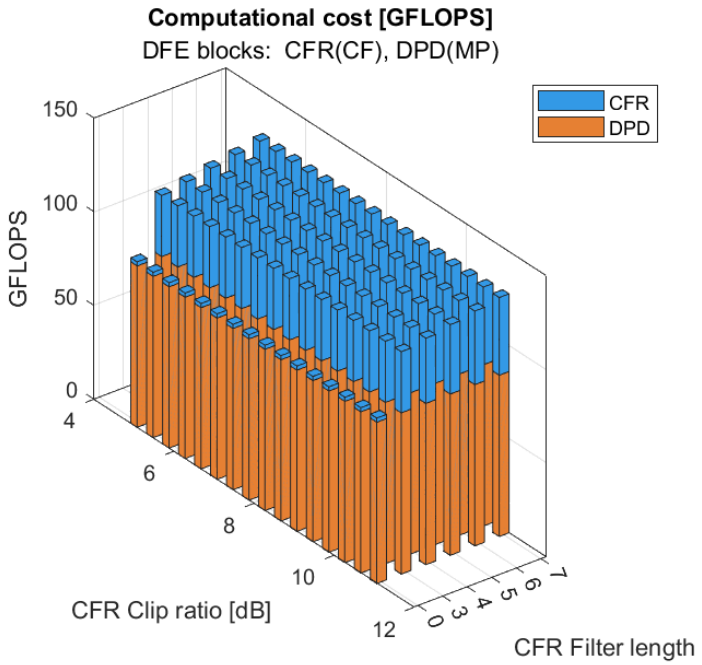

Figure 5.4: Estimated FLOPS as a function of CFR clip ratio and filter length (L_{CFR})

In Figure 5.4 we show the estimated computational complexity for the CFR and DPD blocks, in terms of floating point operations per seconds (FLOPS) calculated via the estimation methods detailed in Chapter 3. Since all DPD parameters are kept constant, the FLOPS originating from that block do not vary. The FLOPS of the CFR block only depend on the filter length and not on the clip ratio as motivated in Chapter 3.

5.2 The effects of varying DPD parameters

In this part of the investigation the parameters in the CFR block are kept constant, and we study the effects of changing the nonlinear order and number of memory taps in the DPD. Table 5.3 below shows the value of the variables that are kept constant.

CFR clip ratio [dB]	CFR filter length
8.2	8

Table 5.3: Constant parameters: Nonlinear order vs. memory depth analysis

5.2.1 Varying maximum nonlinear order and number of memory taps

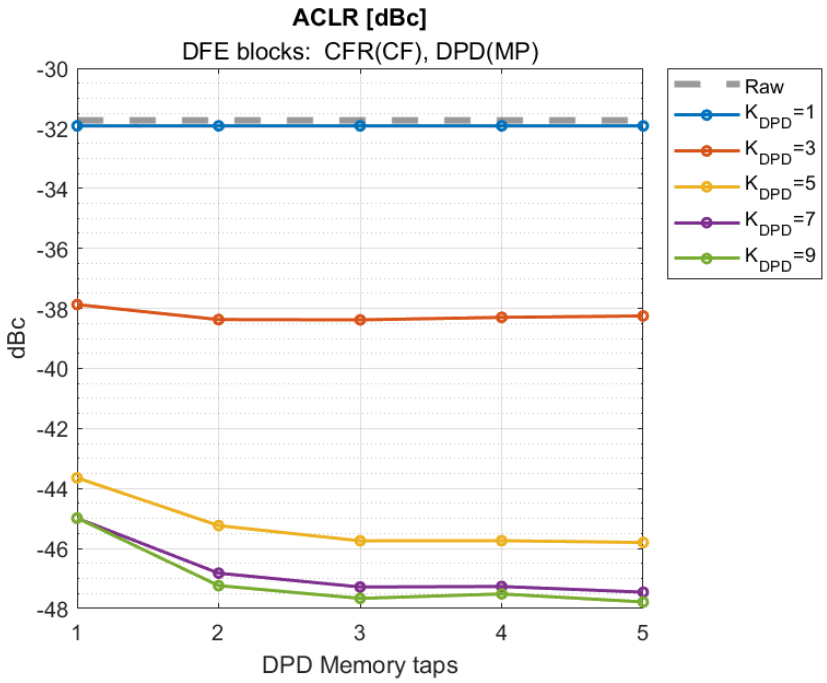

Figure 5.5: ACLR at PA output as a function of nonlinearity order (K_{DPD}) and number of memory taps.

Figure 5.5 clearly shows that increasing the NLO drastically improves ACLR with stagnation for orders 7 and 9. As for the number of memory taps, the algorithm shows some advantages of using more memory taps, especially for higher nonlinear orders. The gain flattens out above 4-5 memory taps which makes sense considering the simulated PA model.

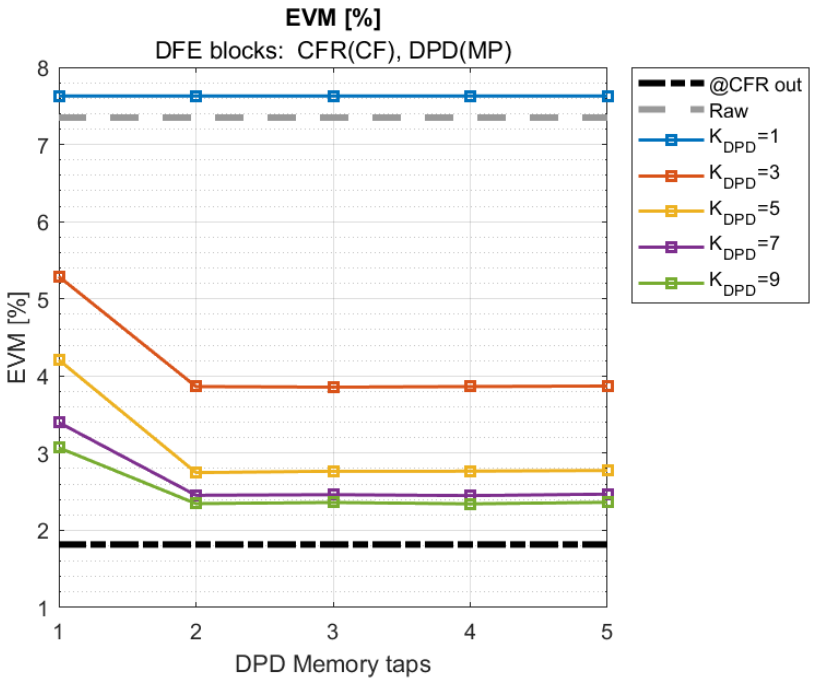

Figure 5.6: EVM at PA output as a function of nonlinearity order (K_{DPD}) and number of memory taps.

When the nonlinear order is low, the EVM performance is poor, but it improves rapidly until order 5, then it stagnates for orders 7 and 9. When it comes to memory taps, they barely affect the EVM for a number of taps greater than 2.

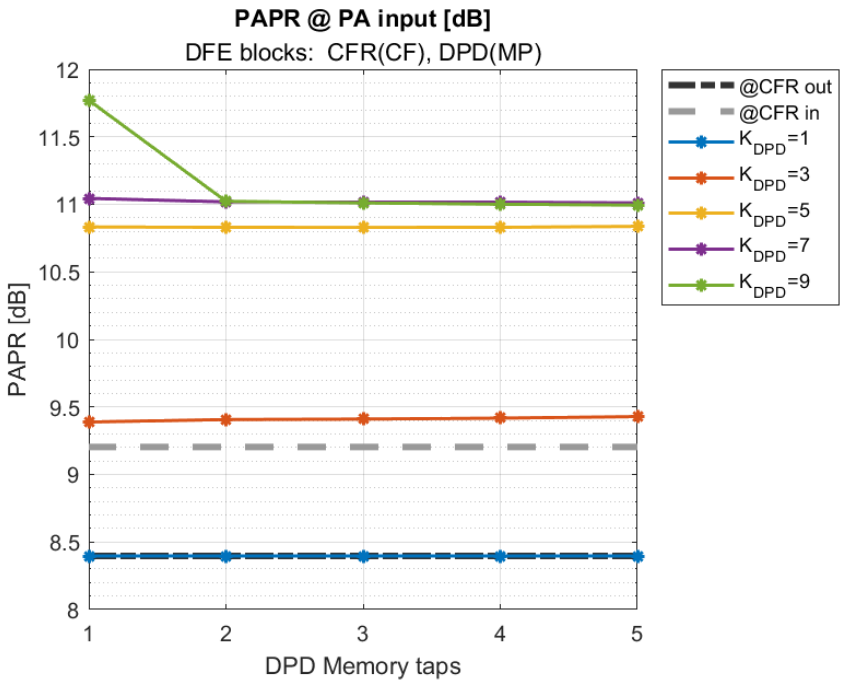

Figure 5.7: PAPR at PA input as a function of nonlinearity order (K_{DPD}) and number of memory taps.

Figure 5.7 shows the effects of nonlinear order on PAPR, where it is visible that higher nonlinear order causes larger expansion of the peaks, leading to higher PAPR, while the number of taps seems to have negligible effects on the PAPR.

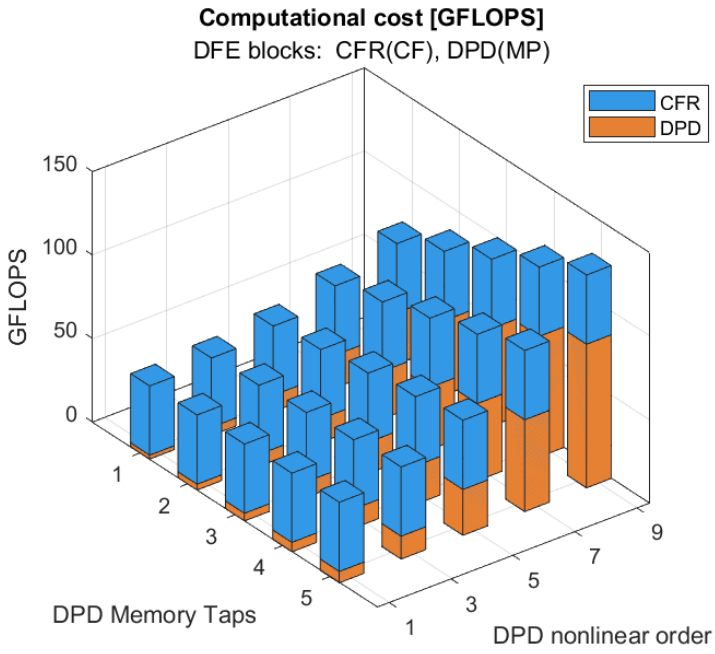

Figure 5.8: Estimated FLOPS as a function of nonlinearity order and number of memory taps.

The computational cost originating from the CFR block is constant since none of those variables are varied. The cost originating from the DPD block increases with nonlinear order and with the number of memory taps as expected from the employed computational complexity models.

5.3 Joint parameter exploration for DPD and CFR

5.3.1 CFR clip ratio vs DPD nonlinear order

What happens when parameters across the CFR and DPD blocks are varied? To start of with, the two most impactful variables of each block are studied, which are clip ratio for the CFR and nonlinear order for the DPD. Table 5.4 below shows the values of the parameters that are kept constant.

DPD number of memory taps	CFR filter length
7	8

Table 5.4: Constant parameters: nonlinear order vs. clip ratio analysis

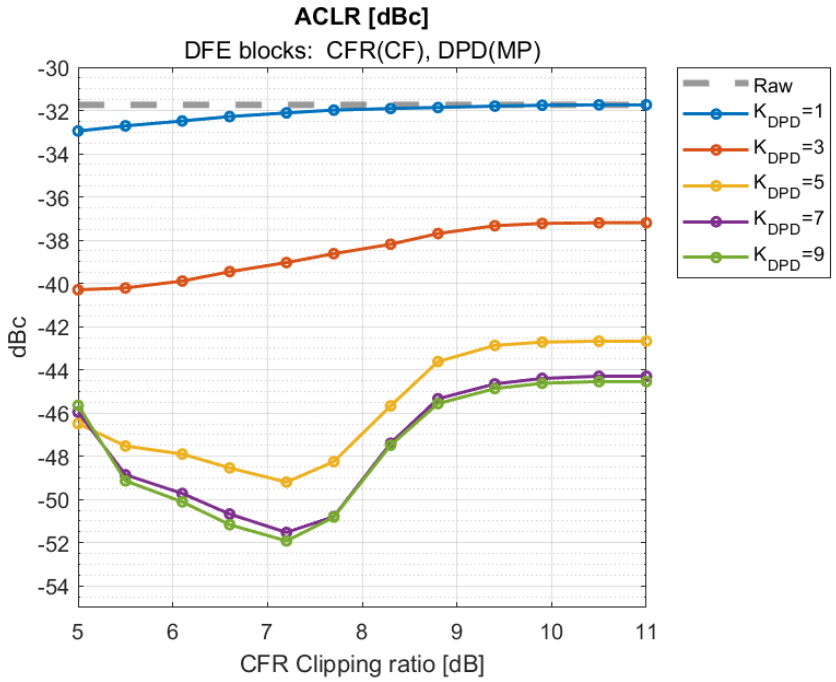

Figure 5.9: ACLR at PA output as a function of DPD nonlinear order (K_{DPD}) and CFR clip ratio.

The lower the clipping ratio, the more of the signal is clipped, resulting in more leakage to the adjacent channels, which is shown in Figure 5.9. When $K_{DPD} = 1$ (the DPD is behaving like a linear system), and the clip ratio is too high for any of the signal to be clipped, the leakage is the same as if the signal were just to be sent straight through the PA without any processing. Increasing the nonlinear order gives a dramatic improvement to the leakage suppression in this region until $K_{DPD} = 7$ where there progress stagnates. This is a sign that the 9th order nonlinear behaviour of the employed PA model is weak and that the PA model can be linearized with a 7th order DPD with good performance. Conversely, if the order of the DPD model is too low compared to that of the PA, it will fail to linearize the PA. When considering high nonlinear order the main

source of ACLR comes from the clipping stage, where the clipped signal yields sharp edges in the time domain. These give rise to higher order terms in the frequency domain which cause spectral regrowth outside the desired channel, setting an upper bound on achievable ACLR suppression.

However, sending an incorrectly distorted signal through the PA's nonlinear region also causes leakage outside the assigned channel.

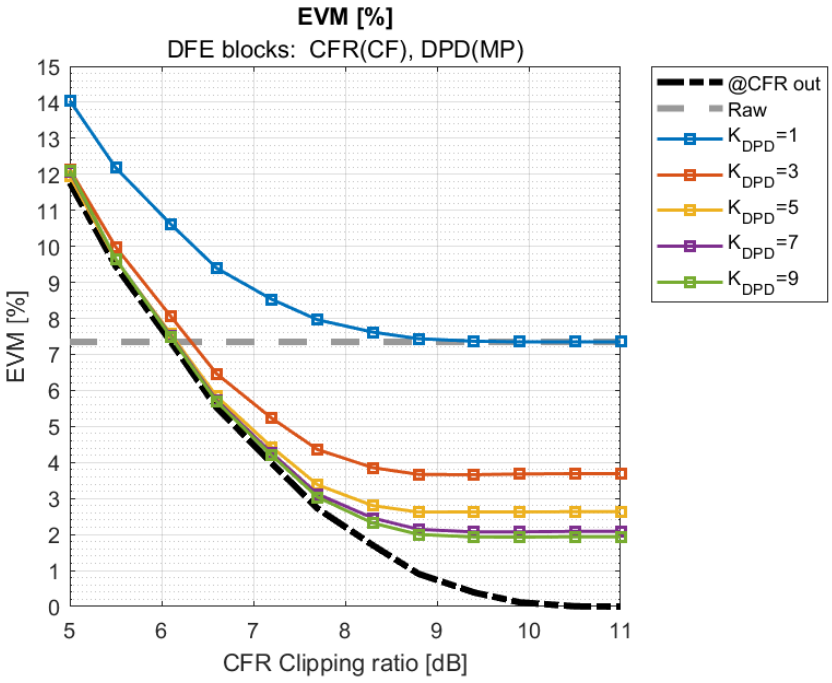

Figure 5.10: EVM at PA output as a function of DPD nonlinear order (K_{DPD}) and CFR clip ratio.

Figure 5.10 shows that the EVM and ACLR show similar behaviour for $K_{DPD} = 1$. When $K_{DPD} = 1$, the DPD cannot compensate for any nonlinearity caused by the PA. Therefore, the lowest error for that curve corresponds to not applying any nonlinear processing to the signal and just sending it straight through the PA. Increasing the nonlinear order of the DPD model drastically improves the EVM with stagnation after $K_{DPD} = 7$ yet again hinting at the PA's nonlinear behaviour being of order 7. Figure 5.10 also shows us the EVM of the signal before arriving to the DPD block. When there is no clipping, there is no error, as expected. As the threshold is lowered and the signal starts to get clipped, the EVM starts to grow. What is noteworthy is that the difference in EVM between the semi-raw signal after CFR and the curves corresponding to the EVM of the distorted signals diminishes rapidly as the signal is clipped more aggressively. For instance even when the modelled nonlinear order is low (e.g., $K_DPD = 3$), the difference in EVM is negligible especially with more aggressive clip ratios. This is because the signal has been clipped so hard that it is mainly distributed within the linear region of the PA and thus has very little nonlinear behaviour to be modelled by the DPD.

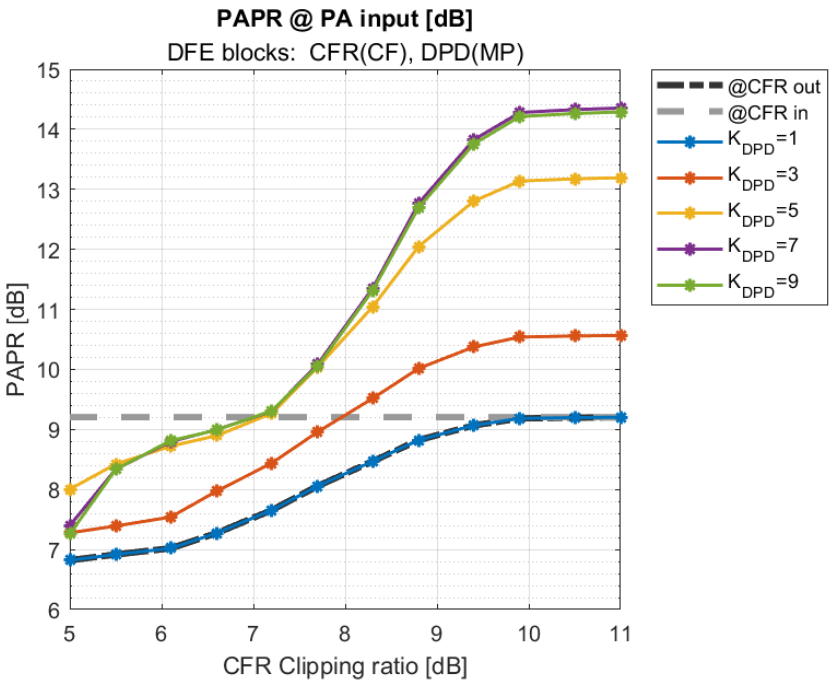

Figure 5.11: PAPR at PA input as a function of DPD nonlinear order (K_{DPD}) and CFR clip ratio.

In figure 5.11 it is shown that $K_{DPD} = 1$ causes no PAPR expansion with respect to the output signal of the CFR, as expected. The other curves corresponding to higher nonlinear orders shows the expansion effects of different nonlinear models of the DPD on the predistorted signal. As expected, clipping the signal more aggressively results in a lower PAPR which is the whole purpose of the CFR block.

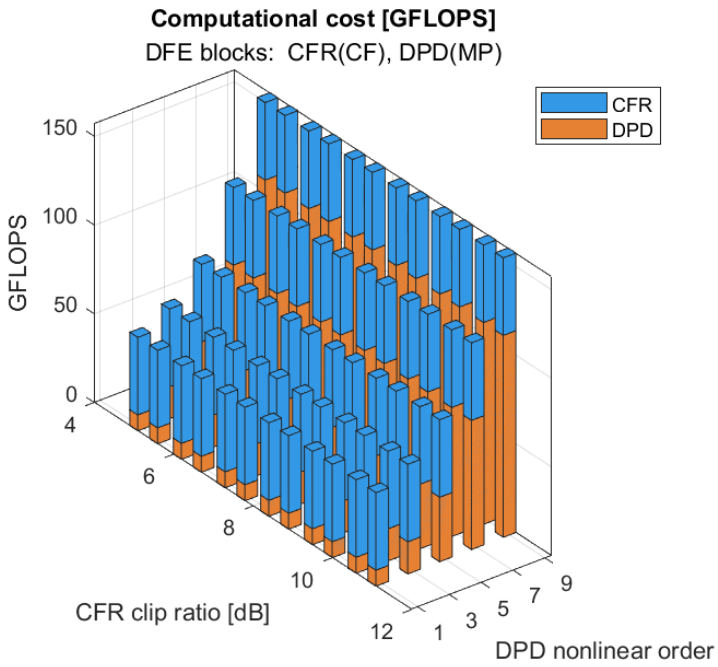

Figure 5.12: Estimated FLOPS as a function of DPD nonlinear order (K_{DPD}) and CFR clip ratio.

Figure 5.12 shows that the computational cost does not depend on the clip ratio, but only on the maximum nonlinear order of the DPD model. When analysing the ACLR, EVM and PAPR performances it is evident that the relative improvement when going from $K_{DPD} = 7$ to $K_{DPD} = 9$ is virtually nonexistent wheras there is a substantial increase in computational cost. This hints at the fact that the optimization will favour solutions with $K_{DPD} = 7$.

5.3.2 CFR clip ratio vs number of DPD memory taps

Table 5.5 below shows the values of the parameters that are kept constant in this scenario.

DPD maximum nonlinear order	CFR filter length
9	8

Table 5.5: Constant parameters: clip ratio vs. number of memory taps analysis

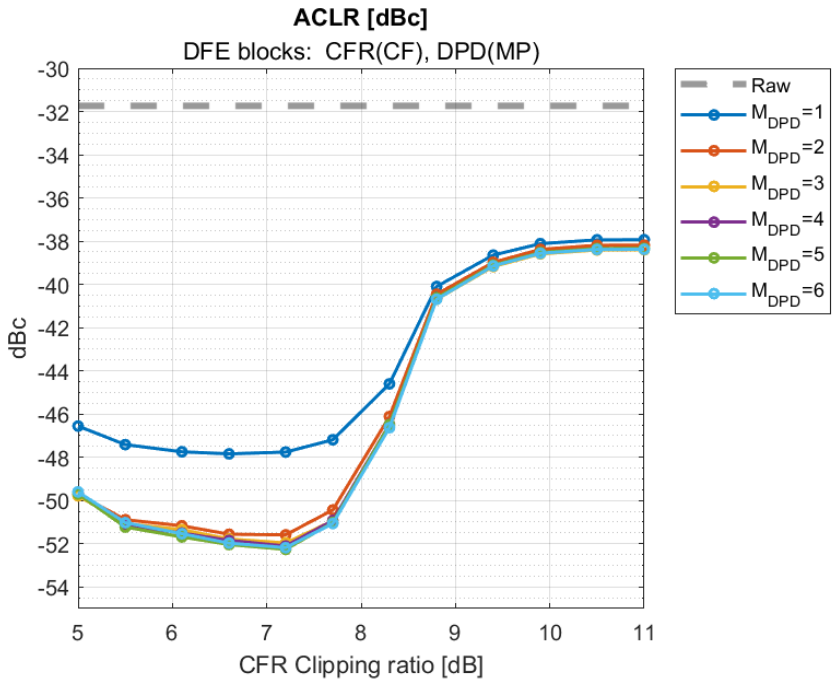

Figure 5.13: ACLR at PA output as a function of number of memory taps in the DPD and CFR clip ratio.

In accordance with the previous simulations, the ACLR shows a convex behaviour which is due to:

- When there is not enough CFR peak reduction, the PAPR of signal explodes leading to high compression at the PA level, which leads to worse ACLR. In this region we are also likely to see the effects of the ACLR degradation due to hard-limiter stage set before the PA.
- When the CFR clipping ratio is too aggressive, the ACLR worsens again due to increased clipping noise despite the CFR filtering. Increasing the number of memory taps reduces leakage, but the improvement stagnates after $M_{DPD} = 3$.

When the CFR clipping ratio is too aggressive, the ACLR worsens again due to increased clipping noise despite the CFR filtering. Increasing the number of memory taps reduces leakage, but the improvement stagnates after $M_{DPD} = 3$.

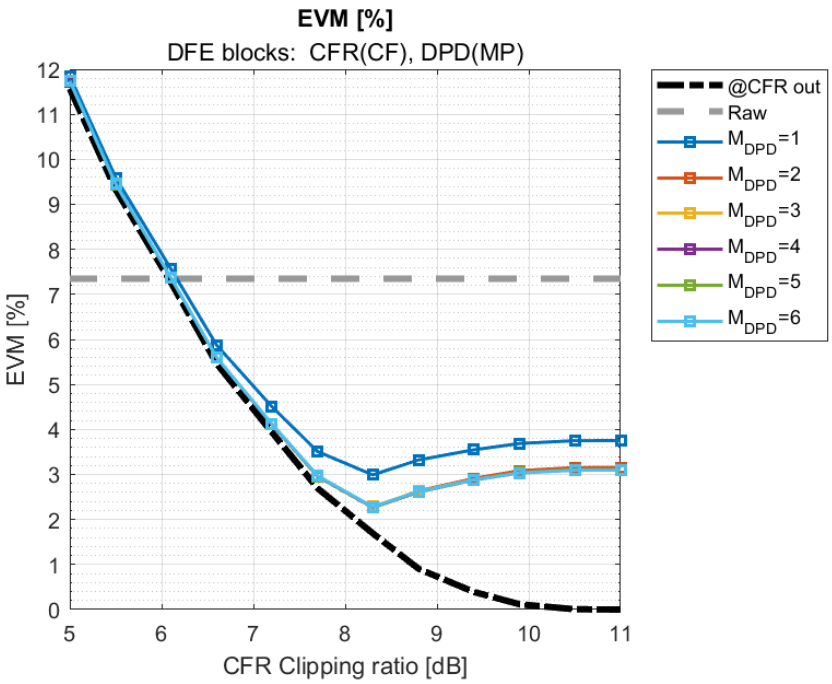

Figure 5.14: EVM at PA output as a function of number of memory taps in the DPD and CFR clip ratio.

When the signal is clipped harder, the EVM increases, just as expected. When it comes to memory depth, a small difference can be seen when there is no clipping where the greater memory depths perform slightly better.

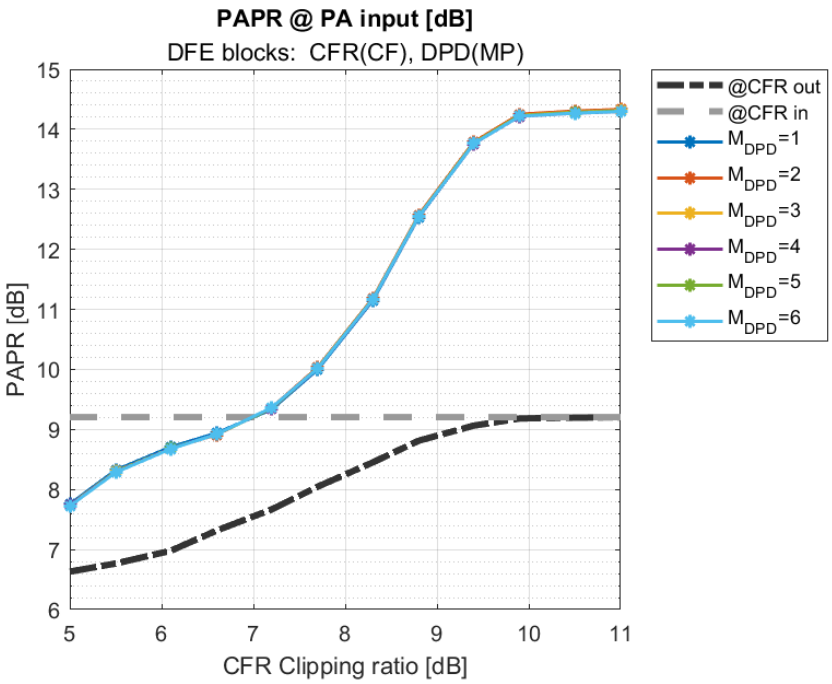

Figure 5.15: PAPR at PA input as a function of number of memory taps in the DPD and CFR clip ratio.

Figure 5.15 shows that, as intended, when the signal is clipped harder, the PAPR decreases. Looking at the part where there is no clipping, the PAPR of the signal is the same before and after the CFR block, as expected. After the signal has passed through the DPD however, the PAPR is worsened. The discrepancy before and after the DPD block decreases with harder clipping. This might be due to the fact that fewer samples will reach the PA's nonlinear region and therefore fewer samples will need to be distorted in the DPD. It seems that varying memory depth does not affect the PAPR since all curves overlap.

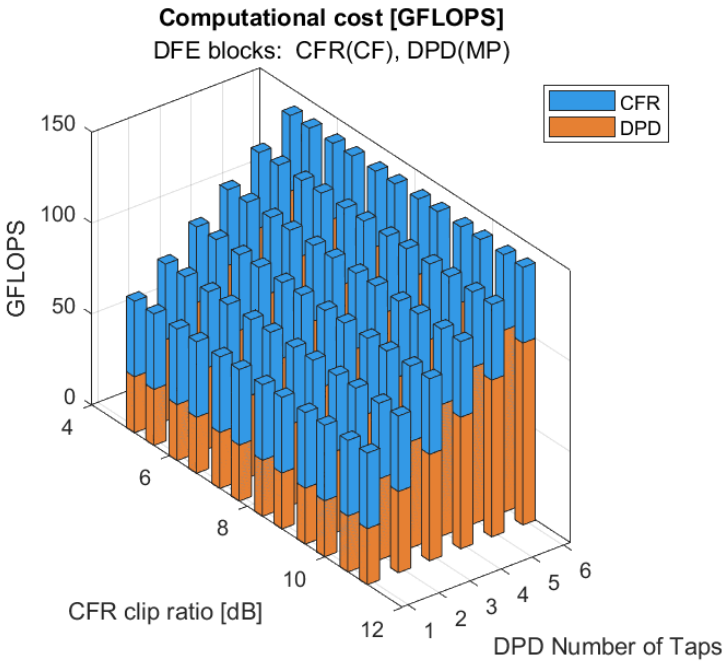

Figure 5.16: Estimated FLOPS as a function of number of memory taps in the DPD and CFR clip ratio.

Figure 5.16 shows that the computational cost does not vary with clip ratio and increases with memory depth. Since the ACLR is barely improved past a memory depth of 3, the optimizer will favour these solutions over higher memory depths.

5.3.3 CFR filter length vs DPD memory taps

Table 5.6 below shows the values of the parameters that are kept constant.

DPD maximum nonlinear order	CFR clip ratio [dB]
7	8.2

Table 5.6: Constant parameters: filter length vs. number of memory taps analysis

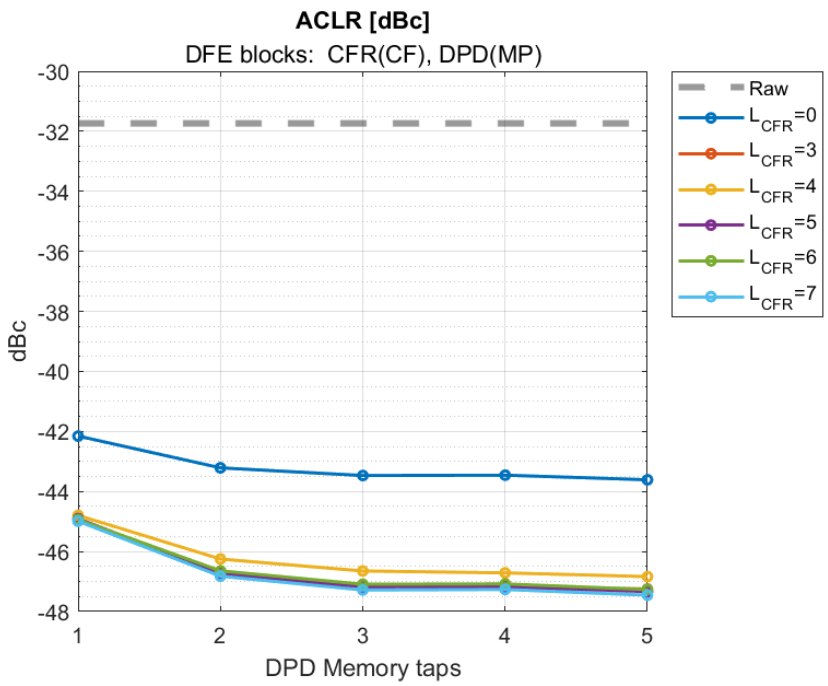

Figure 5.17: ACLR at PA output as a function of CFR filter length (L_{CFR}) and number of memory taps in the DPD.

Figure 5.17 shows that the ACLR is improved when the filter length is increased. The dramatic improvement between $L_{CFR} = 0$ and $L_{CFR} = 3$ showcases the difference in ACLR between not filtering the clipped peaks (hard clipping) and filtering. When it comes to memory taps, there is a slight improvement for the two longest filter with stagnation after the third memory tap. Other than that, the ACLR remains unaffected by changing memory depth.

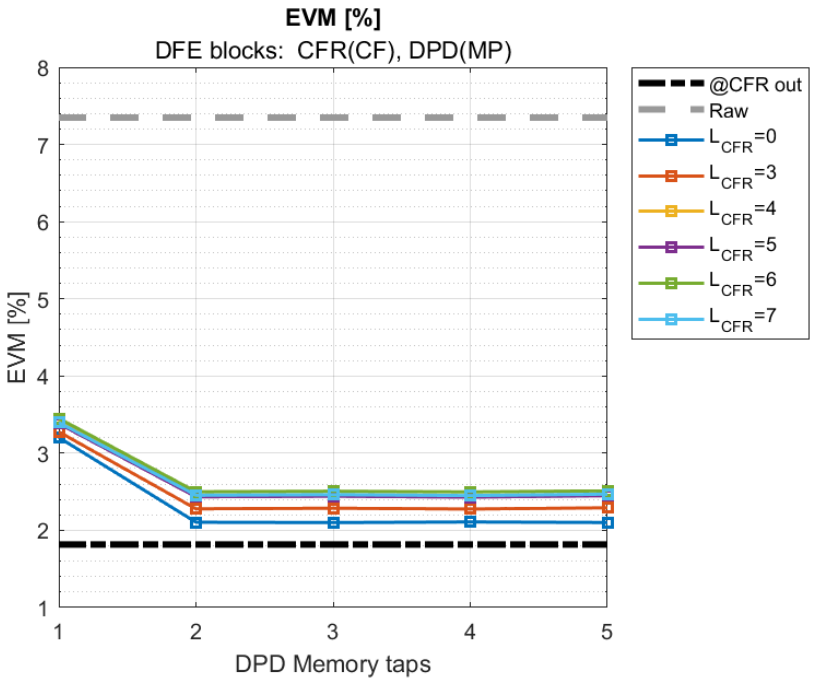

Figure 5.18: EVM at PA output as a function of CFR filter length (L_{CFR}) and number of memory taps in the DPD.

The number of memory taps has negligible effect on EVM when including more than 3 taps. Regarding the effect of CFR filter length, when $L_{CFR} = 0$ it means that the signal is not filtered, meaning that the values of fewer samples are changed thus resulting in a lower EVM. The EVM worsens at $L_{CFR} = 3$ and the rest of the filter lengths result in a similar, higher EVM.

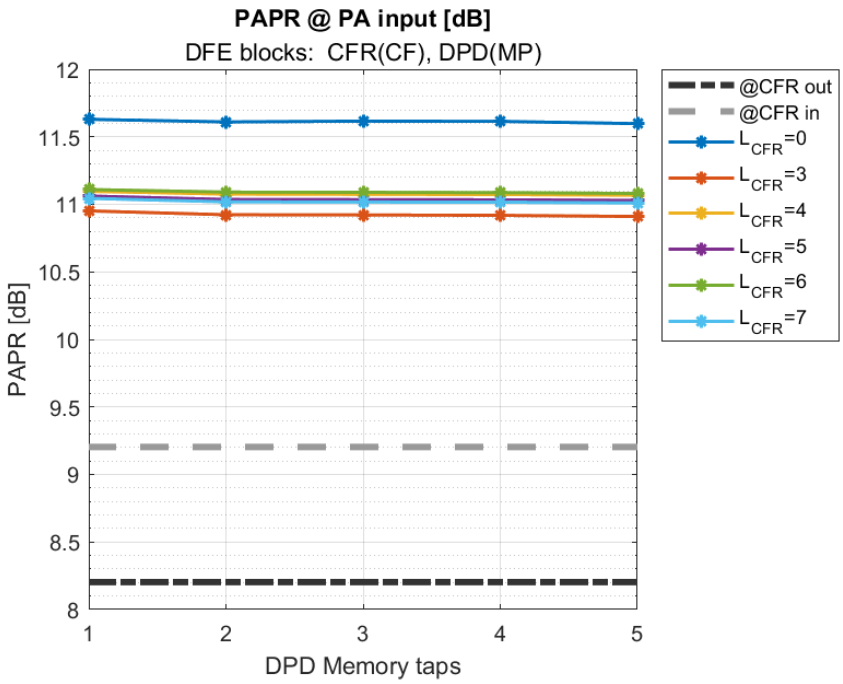

Figure 5.19: PAPR at PA input as a function of CFR filter length (L_{CFR}) and number of memory taps in the DPD.

The PAPR is unaffected by the number of memory taps, while there seems to be a minor impact on the CFR filter length.

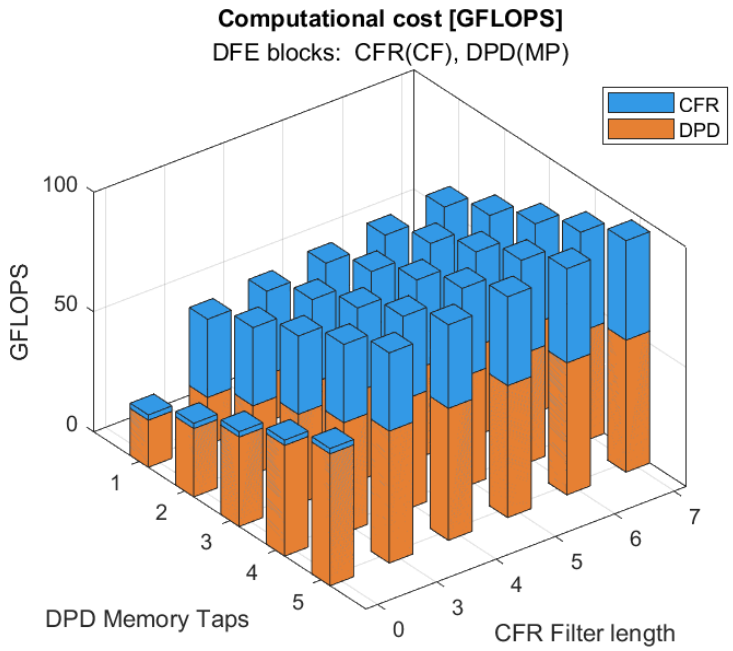

Figure 5.20: Estimated FLOPS as a function of CFR filter length (L_{CFR}) and number of memory taps in the DPD.

The computational cost increases both with memory depth and filter length and the increase is slightly steeper in number of memory taps. The fact that ACLR is more dependent on memory taps than EVM, will be exploited by the optimizer to minimize the amount of taps to satisfy at least the minimum ACLR requirements.

5.3.4 Nonlinear order vs filter length

Table 5.7 below shows what the values of the parameters that are kept constant.

DPD number of memory taps	CFR clip ratio
5	7

Table 5.7: Constant parameters: nonlinear order vs. filter length analysis

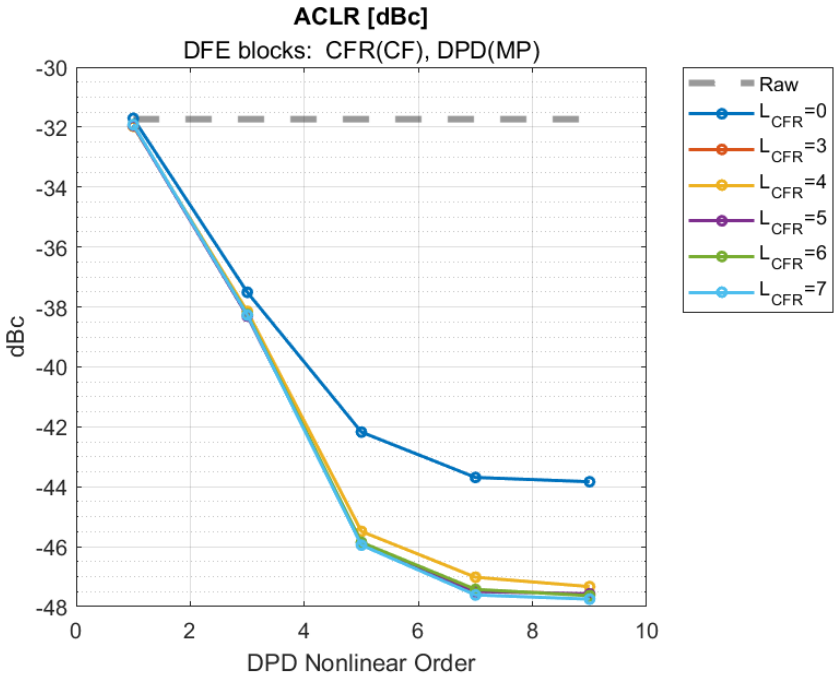

Figure 5.21: ACLR at PA output as a function of nonlinear order and filter length (L_{CFR}).

Increasing the maximum nonlinear order improves ACLR, in accordance with the previous investigations. Similarly, there is a stagnation when the nonlinear order is taken past 7. The overall trend when it comes to filter lengths is that longer filters improve the ACLR. The exception is $L_{CFR} = 0$ which performs about as good as $L_{CFR} = 4$ or $L_{CFR} = 5$. As the nonlinear order decreases, the effect of varying filter length on ACLR becomes less and less impactful. It seems like the larger source of ACLR originates from the DPD blocks ability to correctly model the PA's nonlinear behaviour, which it fails to do adequately for models with lower nonlinearity order. Having longer filters should smooth out the sharp edges caused by the clipping and reduce the out of band spectral regrowth caused by it, thus lowering the baseline ACLR degradation introduced by the CFR.

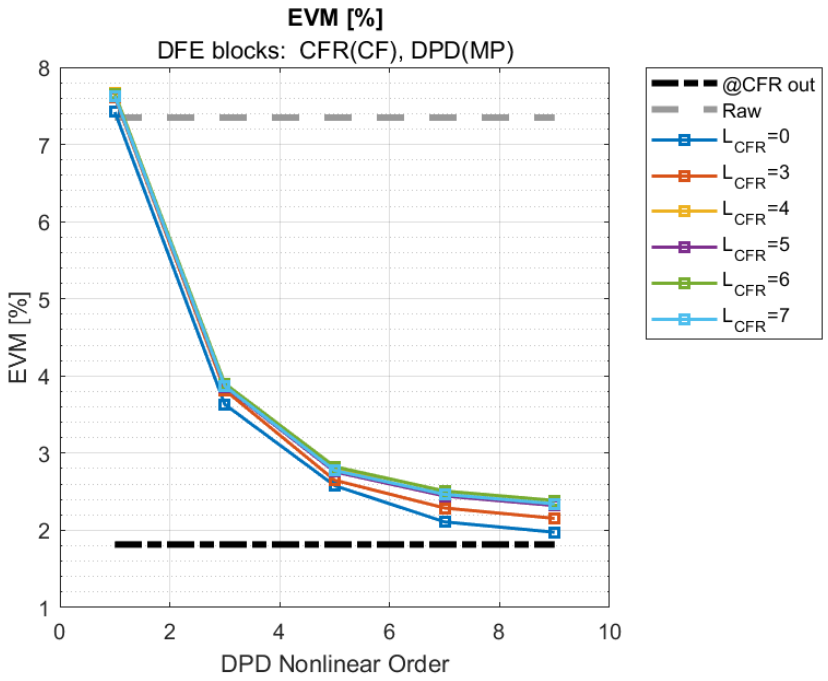

Figure 5.22: EVM at PA output as a function of nonlinear order and filter length (L_{CFR}).

Figure 5.22 shows that not filtering the signal at all results in the best EVM, which makes sense since fewer samples are being manipulated. Longer filters worsen the EVM, but the deterioration stagnates after $L_{CFR} = 3$. The worst EVM is when the DPD model only uses linear terms. It then fails to compensate for the PA's nonlinearity so bad that the error is worse than if the signal was sent straight through without being processed at all. When the maximum nonlinear order is 3 or less, the impact of changing filter lengths is fairly insignificant. For orders above 3, filter lengths becomes more important though.

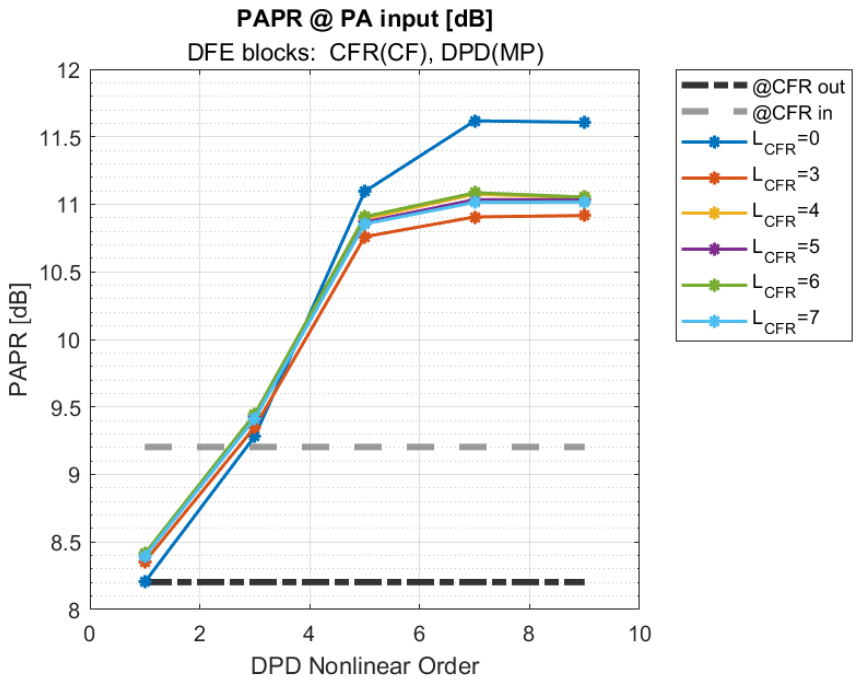

Figure 5.23: PAPR at PA input as a function of nonlinear order and filter length (L_{CFR}).

The shorter the filter, the lower the PAPR, with the exception of not filtering at all. Supposedly the unfiltered clipping noise from the CFR causes the clipped peaks to regrow when predistorted via higher-order DPD models. Increasing the nonlinear order from 1 to 5 causes the PAPR to increase slightly, while above that the impact is negligible.

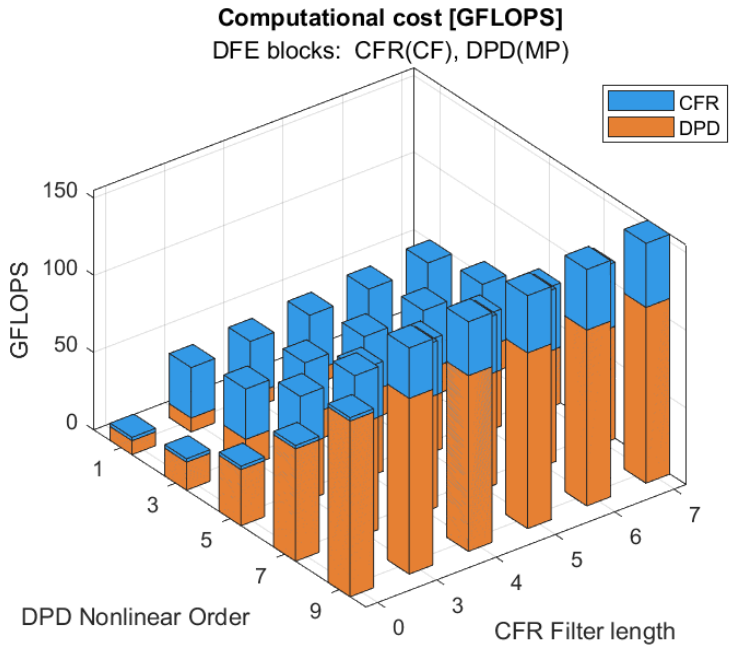

Figure 5.24: Estimated FLOPS as a function of NLO and filter length (L_{CFR}).

The increase in computational cost is a lot steeper with increasing nonlinear order than filter length. This means that if increasing the filter length one step or increasing the nonlinear order one step both improve the performance by the same amount, the optimizer would choose to increase the filter length.

5.4 Extended parameter exploration: Hard limiter vs CFR clip ratio

The CFR block is not always perfect meaning that some filtered samples might exceed the clipping threshold when entering the DPD section. This is due to the filtering operated at the CFR level, and/or to the interpolation performed by the up-sampler before the DPD. In order to circumvent this, a hard limiter is introduced as shown in Figure 5.25 below.

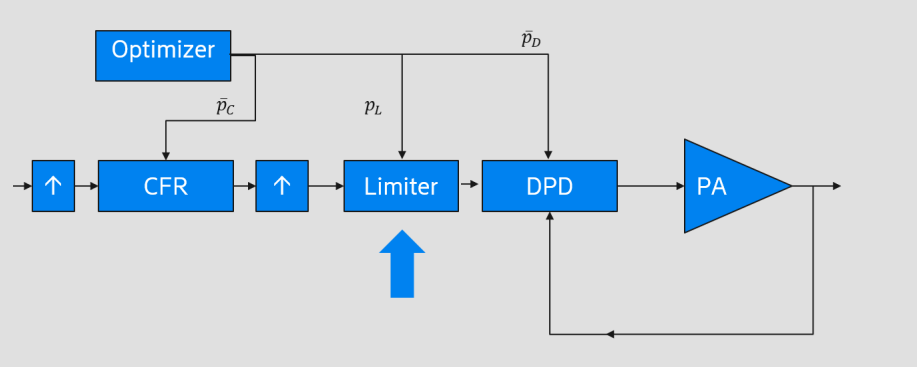

Figure 5.25: Extended DFE chain including hard limiter block and proposed parameter optimization.

In this investigation, the hard limiter is configured with a threshold that is relative to the CFR threshold, expressed in dB. Table 5.8 below shows the values of the parameters that are kept constant.

DPD filter length	DPD memory taps	DPD nonlinear order
8	7	7

Table 5.8: Constant parameters: Hard-limiter clipping ratio vs. CFR clipping ratio

In Figures 5.26, 5.27 and 5.28, four curves are plotted representing the relative clip ratio (CR_{HL1}) of the hard limiter with respect to the one used in the CFR. These plots have the CFR clip ratio on the x-axis and the performance metric on the y-axis. A percentage is displayed next to each data point, representing the share of samples affected by the hard clipper. This value increases as the signal is clipped more aggressively. This is because the imperfect CFR block will have to handle a larger share of the samples meaning that it will leave more samples above the threshold due to peak regrowth. This can also be mitigated by increasing the number of stages in the multi-stage CFR algorithm. The purple curve ('off') represents not having a hard limiter at all. The red curve ($CR_{HL1} = 0$ dB) corresponds to the hard limiter's threshold being the same as that of the CFR block. The blue curve ($CR_{HL1} = -1$ dB) represents the case where: $\theta_{HL} = 0.79 \cdot \theta_{CFR}$ and the yellow curve ($CR_{HL1} = 1$ dB) represents the case where: $\theta_{HL} = 1.26 \cdot \theta_{CFR}$, with θ_{HL} clipping threshold of the hard limiter and θ_{CFR} clipping threshold of the CFR.

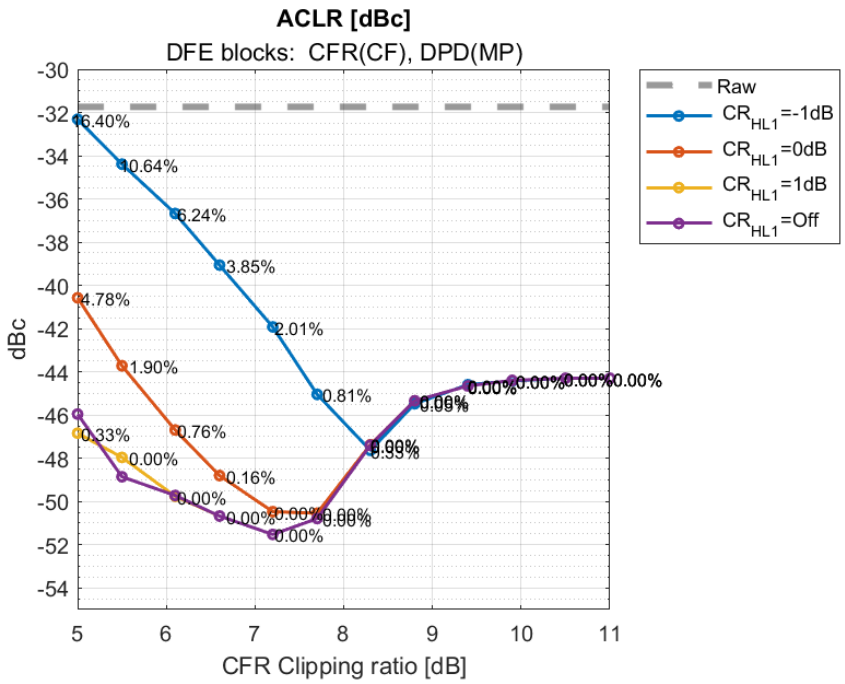

Figure 5.26: ACLR at PA output as a function of CFR clip ratio and relative clipping ratio of the hard limiter (CR_{HL1}).

The curves of Figure 5.26 overlap almost perfectly as long as no samples need to be handled by the hard limiter. The blue curve represents having a 1 dB lower threshold than that in the CFR, meaning that the hard limiter will clip more samples compared to the other cases It also means that the hard limiter engages earlier when lowering the CFR threshold. Since the hard limiter cuts more peaks, there are more sharp edges in the time domain which leads to higher spectral regrowth outside the assigned channel, ultimately resulting in a higher ACLR. The red curve represents having an identical threshold in the hard limiter and in the CFR block. The phenomenon of peak regrowth, causing the 0 dB hard limiter to clip peaks regenerated by the CFR filter and up-sampler, is visible for CFR clip ratios lower than, 7 dB. Just as before, more samples clipped by the hard limiter results in a worse ACLR. The yellow curve corresponds to setting the HL threshold 1 dB higher than that in the CFR block. This means that the hard limiter will actually let through some of the samples above the CFR threshold. Regarding the the 1 dB curve, the phenomenon of peak regrowth has to be large for the hard limiter to be engaged, and this happens only when the CFR threshold is lowered further. This curve has significant overlap with the purple one (hard-limiter switched off).

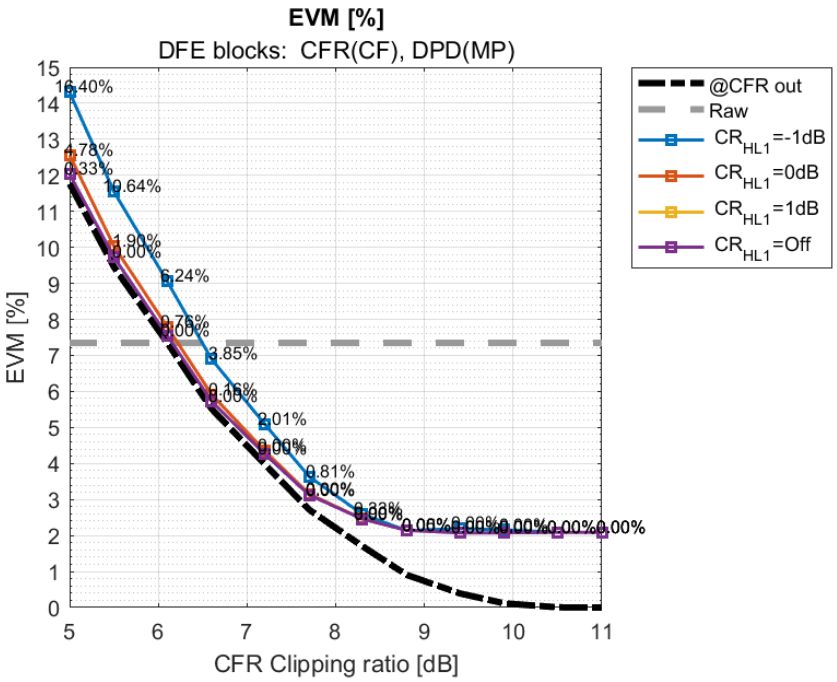

Figure 5.27: EVM at PA output as a function of CFR clip ratio and relative clipping ratio of the hard limiter (CR_{HL1}).

The yellow and the purple curves of Figure 5.27 overlap indicating that the few samples handled by the "tolerant" limiter do not significantly affect the EVM. As before, the blue curve represents the "stricter" limiter, and it results in the worst EVM performance. The red curve illustrates the EVM caused by clipping the residual samples above the CFR threshold. This impact is not that large compared to not having any hard limiter block at all. Few samples are affected, and their modification is relatively small.

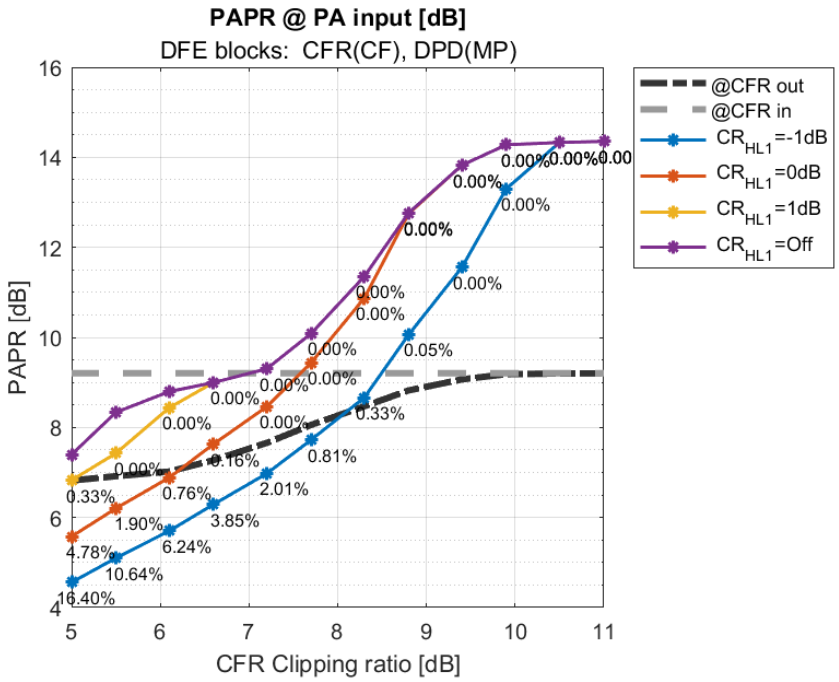

Figure 5.28: PAPR at PA input as a function of CFR clip ratio and relative clipping ratio of the hard limiter (CR_{HL1}).

When it comes to PAPR, there is a similar but complementary behaviour to that of ACLR. The difference here being that more samples handled by the hard clipper result in lower PAPR, which is as expected. The blue curve represents the case where the largest share of peaks are clipped, resulting in the lowest peak-to-average power ratio. The hard limiter represented by the red curve only clips the residual samples above the CFR threshold, which is far fewer than the yellow one. The yellow curve overlaps with the purple one the longest meaning that the limiter is engaged the least and therefore affects the PAPR the least.

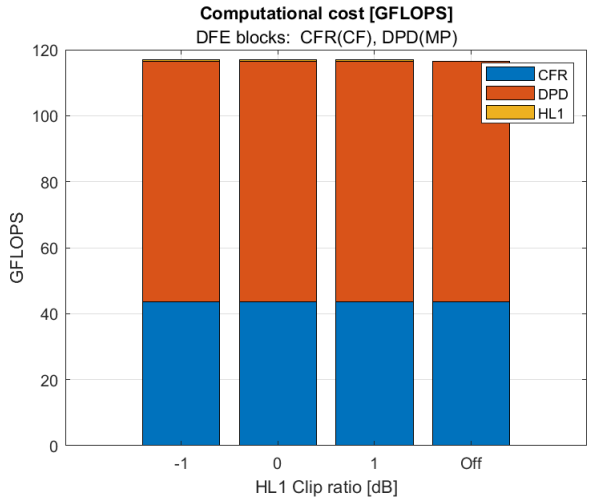

Figure 5.29: Estimated computational complexity of the DFE blocks (CFR, DPD, hard limiter)

Figure 5.29 shows the computational complexity of the DFE chain including CFR, DPD and hard limiter. As only clip ratios are varied, the estimated complexity stays the same, while we also see that the complexity of the hard limiter is negligible (barely visible top yellow bars) when compared to the DPD and CFR.

5.5 Joint parameter optimization

5.5.1 Exploration of CFR/DPD four-dimensional parameter space

In the previous sections the influence of CFR and DPD parameters variation has been studied for a couple of parameters. In this section they will be varied all at once. The simulator described in Chapter 4 is used to estimate the performance metrics and computational cost for each candidate parameter vector. The metrics are then compared to a set of constraints, described in the optimization problem of Section 3.1, to determine the feasibility of the specific solution. The values used to set those constraints are based on [1] and are: $\text{EVM}_{lim} = 3.5\%$, $\text{ACLR}_{lim} = -46$ dBc, $\text{PEP}_{high} = -8$ dB, $P_{high} = -18.9$ dB, and $P_{low} = -19.1$ dB.

Finally, the objective function defined in Section 3.2 is used to rank the feasible solutions and select the best one.

CFR: Clip ratio (dB)	5-10
CFR: Filter length	0, 3-10
DPD: Nonlinear order	1,3,5,7,9
DPD: Number of memory taps	1-7
Hard limiter	off

Table 5.9: Varying and constant parameters for the four-variables analysis

Vizualizing four variables at the same time is tricky since there are only three spatial dimensions to work with. One variable (CFR filter length) has been omitted from the figures below since it had limited impact on the performance metrics during the dual parameter variation.

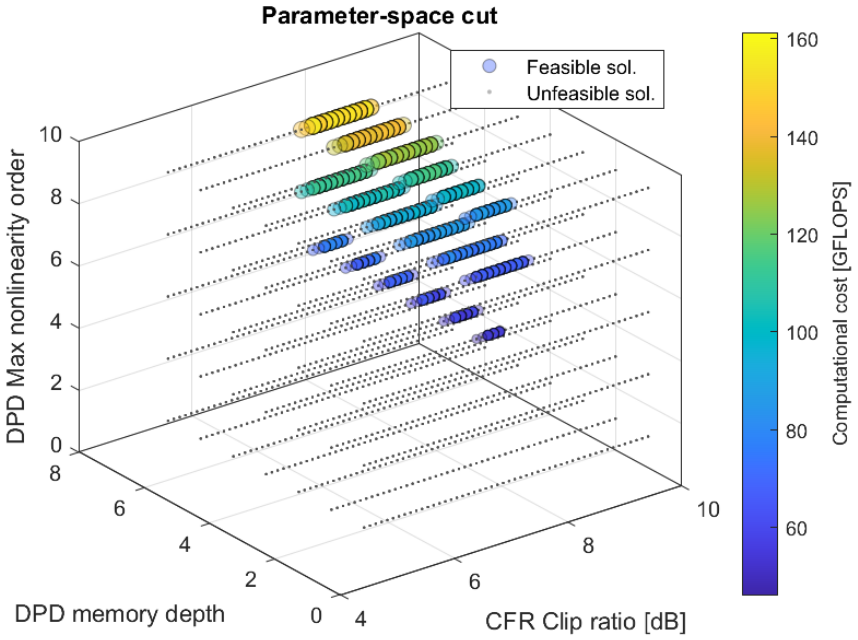

Figure 5.30: Parameter-space cut with respect to CR, NLO and number of memory taps.

Figure 5.30 above shows the set of feasible solutions in the parameter space spanned by the variables memory depth, maximum nonlinearity order of the DPD model and the CFR clip ratio. If the combination of these three parameter values leads to a feasible solution, a bubble is plotted in that point in space. The colour of the bubble represents the computational cost of this solution. If the parameters generate a result that violates the constraints in Chapter 3.2, it is marked with a small black dot. The feasible region seems to be compact within a well-defined range of CFR clip ratios (continuous parameter), and DPD memory depth/nonlinearity order (discrete parameters). The feasible region gets a bit thinner as memory depth decreases meaning that shallower memory depths lead to fewer feasible solutions.

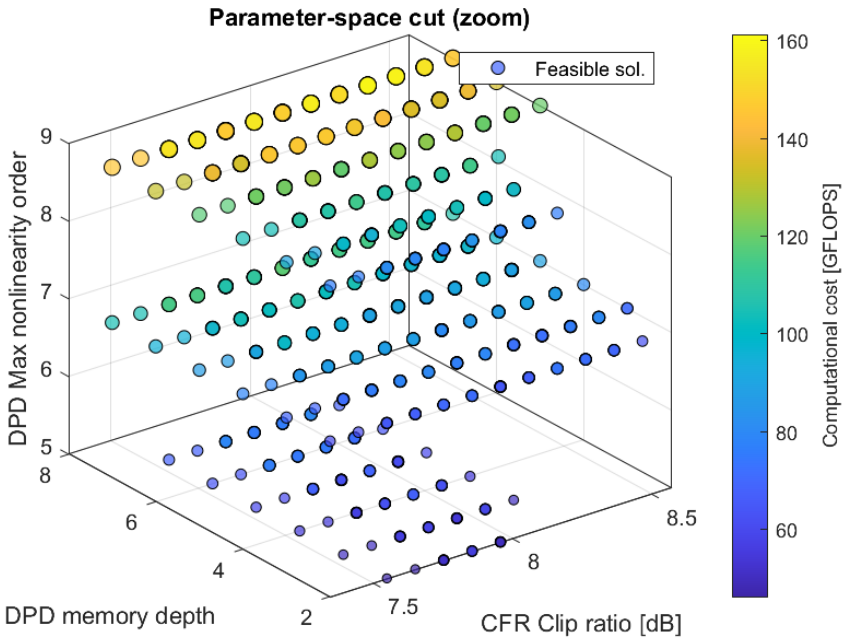

Figure 5.31: Parameter-space cut with respect to CR, NLO and number of memory taps, centered on feasible solutions.

Figure 5.31 above is the same as Figure 5.30, only zoomed in on the feasible solutions. The cross-section for a nonlinear order of 7 is the widest, meaning that this region the most tolerant to variations in clip ratio and memory depth. However, these points do not result in the lowest computational cost. The computational complexity increases drastically with memory depth and nonlinear order as expected.

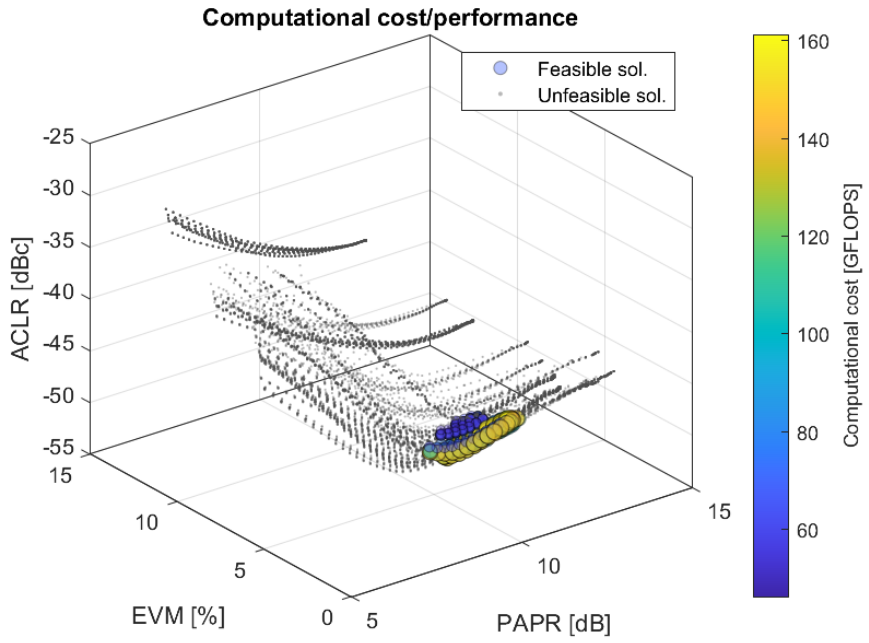

Figure 5.32: Performance metrics (EVM, ACLR, PAPR) and associated DFE computational cost explored over a constrained four-dimensional parameter space.

The performance metrics of the complete grid-based exploration over the selected parameter space is plotted in Figure 5.32. The pattern looks a bit like "hairs blowing in the wind". The "hairs" are made up of around 50 dots along a trajectory. The clip ratio is varied between 5 dB and 10 dB using 50 data points, which suggests that a "hair" corresponds to varying the clip ratio and keeping all other parameters constant. Clusters of "hairs" or "locks" can be identified. These are characterized by a group of "hairs" that converge to a point. When zooming in on the dots that make up a hair, it becomes apparent that each dot is made up of a cluster of individual data points. These small clusters are probably formed when clip ratio and maximum nonlinear order are kept constant, and the parameters filter length and memory depth are varied. The reasoning behind this is that the two latter parameters produce similar results for most of the values they take (see Section 5.3.3). In other words, there are many scenarios when varying filter length and memory depth that produce little to no difference on the performance metrics, and those solutions are therefore represented by closely spaced points in the parameter space.

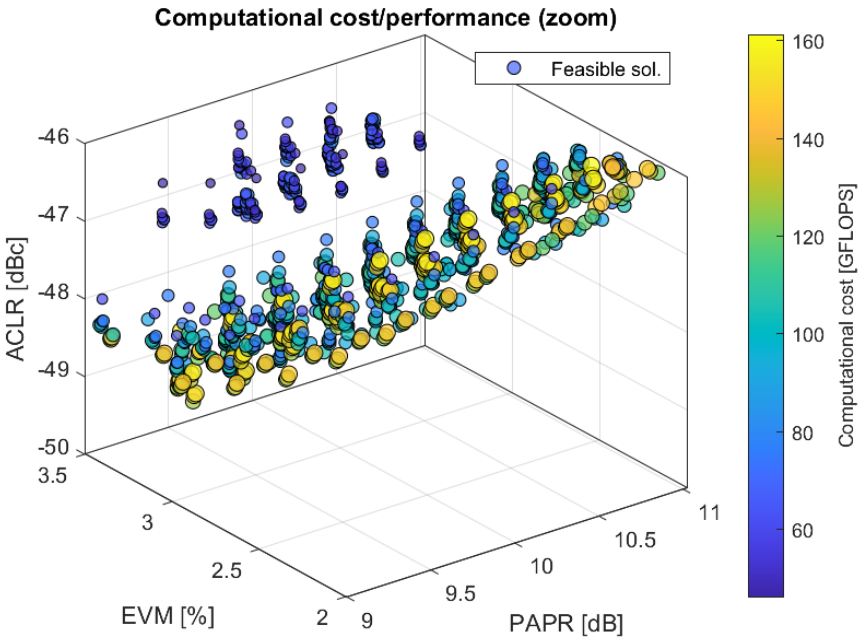

Figure 5.33: Performance metrics (EVM, ACLR, PAPR) and associated DFE computational cost explored over a constrained four-dimensional parameter space.

When taking a closer look at the feasible solutions it can be seen that the best solutions when it comes to computational cost tend to be the one with worst ACLR and EVM. Nevertheless, there are several feasible solutions with relatively low computational cost which still satisfy constraints on ACLR, EVM and PAPR with some margin. In the next chapter, the proposed objective function is used to find those solutions according to the desired composite cost metric.

5.5.2 Joint CFR/DPD constrained optimization in four dimensional parameter space

If one only valued low computational cost, selecting the best parameters would be easier, all one needs to do is select the cheapest feasible solution and the problem would be solved. Doing this however means that the solution would probably lie just at the edge of acceptable EVM and ACLR with little to no margin.

In order to take this aspect into account, an objective function is introduced as explained in Chapter 3. The objective function contains three different parameters a, b and c, which dictate the importance of low computational cost, low EVM and low ACLR respectively. An example of how to interpret these three parameters is given at the very end of Chapter 3.

The tables below contain results from the same simulation, but with different weight factors in the objective function. The simulation gave 1073 feasible solutions, over an explored parameter grid composed by 15 751 points, which are presented in a list sorted by value of the objective function in ascending order. The limit on EVM is 3.5%, the limit on ACLR is -46 dBc and the reference level for computational cost is 50 GFLOPS. The first five rows show the best results (minimum value encountered for the objective function), then a result from the middle of the list is shown, and, finally the worst solution is presented.

Cost	GFLOPS	EVM[%]	ACLR[dBc]	CR [dB]	Fil Len	NLO	Mem
2.6870	60.549	2.8724	-47.835	7.7551	3	7	2
2.6878	60.549	2.7520	-47.608	7.8571	3	7	2
2.6988	60.549	2.6460	-47.356	7.9592	3	7	2
2.7011	60.549	3.0051	-47.996	7.6531	3	7	2
2.7166	62.761	2.9781	-48.143	7.8571	4	7	2
-	-	-	-	-	-	-	-
3.4222	90.902	2.6402	-47.136	8.0612	5	9	3
-	-	-	-	-	-	-	-
4.8747	161.26	2.2798	-46.008	8.4694	10	9	7

Table 5.10: Best, mid-range and worst values for the objective function ($a = b = c = 1$) for a grid search over the four-dimensional parameter space: clip ratio, filter length (CFR), and nonlinear order, number of taps (DPD).

The results shown in table 5.10 reflect setting the weight parameters $a = b = c = 1$ in the cost function. This will serve as a baseline for comparison when varying the individual weight parameters afterwards.

A first observation that comes to mind is that the four best solutions all share the same filter length, maximum nonlinear order and memory depth. The only DFE parameter that changes is the clip ratio. This is reasonable though when looking at how the grid for the parameter space is set up. The clip ratio (CR) is a continuous variable and therefore many more discrete sample points were used as opposed to the other three which are discrete and only take on few values in the simulation. The computational cost in GFLOPS has a far greater range than EVM and ACLR which suggests that its weight factor is more impactful than the others when it comes to the rank of the results in the

table. When looking at the entire EVM column, it can be noted that the five best solutions have a rather average EVM suggesting that its weight factor is less impactful than the others. This makes sense since the feasible solutions have a relatively small range in EVM. When it comes to ACLR, it is important to note that it is expressed in logarithmic units. Therefore since the lowest ACLR is -46.62 dBc and the worst -46 dBc, their ratio in linear unit is

$$\text{Ratio}_{ACLR} = 10^{\frac{-46.001+49.619}{10}} = 2.300$$

This is in between the ratios of EVM an GFLOPS as shown in Table 5.11 below. The weight factor in front of ACLR therefore impacts the rank of the results moderately compared to that of EVM and GFLOPS.

	GFLOPS	EVM	ACLR
Max	161.257	3.4955	-46.001 dB
Min	46.264	2.2933	-49.619 dB
Ratio	3.486	1.670	2.300 (lin)

Table 5.11: Maximum, minimum and maximum ratio = (max/min) of target function metrics over the feasible solution space.

It is important to remember from Section 3.2 that no solution can have and EVM or ACLR higher than that set in the constraints, therefore their respective terms in the objective function will never exceed 1 when $a = b = c = 1$. The computational cost however does not determine whether a solution is feasible or not. The parameter C'_{max} can be set pretty arbitrarily. The lower it is set, the more the term contributes to the cost. If this parameter was defined to be the largest computational cost, this term would behave more similarly to the others in that it could never exceed 1 when $a = b = c = 1$. In the simulation in question C'_{max} is set at 50 GFLOPS which is pretty low since it makes this term dominate over the other two. This can all be calibrated by changing the values of a, b and c though.

Cost	GFLOPS	EVM[%]	ACLR[dBc]	CR [dB]	Fil Len	NLO	Mem
3.6440	46.264	3.1755	-46.525	7.7551	3	5	2
3.6446	46.264	3.0707	-46.378	7.8571	3	5	2
3.6571	46.264	3.2937	-46.628	7.6531	3	5	2
3.6585	46.264	2.9813	-46.195	7.9592	3	5	2
3.6832	46.264	3.4253	-46.686	7.5510	3	5	2
-	-	-	-	-	-	-	-
5.2565	91.515	2.4410	-46.465	8.3673	5	7	5
-	-	-	-	-	-	-	-
8.0999	161.257	2.2710	-46.008	8.694	10	9	7

Table 5.12: Best, mid-range and worst values for the objective function ($a = 2$, $b = 1$, $c = 1$) for a grid search over the four-dimesional parameter space: clip ratio, filter length (CFR), and nonlinear order, number of taps (DPD).

Setting $a = 2$, $b = 1$, $c = 1$ emphasizes the importance of solutions with low computational cost, which can clearly be seen in Table 5.12. The five best

solutions selected by the optimizer all correspond to choosing the lowest possible computational cost. Comparing this result to that in Table 5.10, it can be seen that the computational cost for the five best solutions has decreased by roughly 25%. EVM and ACLR on the other hand have worsened and are pushed closer to the tolerable limit. The solution with the highest cost factor is the one with the highest GFLOPS as expected. It is noteworthy however that this solution heavily favours low EVM over low ACLR. The ACLR in this case lies exactly on the edge of what is tolerable while the EVM has wider margin with respect to the selected constraint (3.5%).

Cost	GFLOPS	EVM[%]	ACLR[dBc]	CR [dB]	Fil Len	NLO	Mem
3.4522	60.549	2.5501	-47.056	8.0612	3	7	2
3.4548	60.549	2.6460	-47.356	7.9592	3	7	2
3.4581	60.549	2.4675	-46.772	8.1633	3	7	2
3.4689	60.549	2.3928	-46.503	8.2653	3	7	2
3.4741	60.549	2.7520	-47.608	7.8571	3	7	2
-	-	-	-	-	-	-	-
4.2372	93.727	3.0568	-48.105	7.8571	6	7	5
-	-	-	-	-	-	-	-
5.7469	161.257	3.4955	-48.804	7.5510	10	9	7

Table 5.13: Best, mid-range and worst values for the objective function ($a = 1, b = 2, c = 1$) for a grid search over the four-dimesional parameter space: clip ratio, filter length (CFR), and nonlinear order, number of taps (DPD).

Increasing b from 1 to 2 results in better EVM. There is an overall improvement in EVM in the top five solutions in Table 5.13 compared to Table 5.10. The worst solution in this case selects for the highest EVM and is more lenient on ACLR which makes sense. The computational cost is always the highest possible in the worst solution due how heavily it weighs in the objective function, as discussed earlier.

Cost	GFLOPS	EVM[%]	ACLR[dBc]	CR [dB]	Fil Len	NLO	Mem
3.2816	62.761	3.2828	-48.642	7.6531	4	7	2
3.2892	62.761	3.1238	-48.436	7.7551	4	7	2
3.3001	62.761	3.4559	-48.768	7.5510	4	7	2
3.3271	62.761	2.9781	-48.143	7.8571	4	7	2
3.3326	60.549	3.0051	-47.996	7.6531	3	7	2
-	-	-	-	-	-	-	-
4.1391	80.456	2.4808	-46.407	8.3673	8	7	3
-	-	-	-	-	-	-	-
8.8729	161.257	2.2798	-46.008	8.4694	10	9	7

Table 5.14: Best, mid-range and worst values for the objective function ($a = 1, b = 1, c = 2$) for a grid search over the four-dimesional parameter space: clip ratio, filter length (CFR), and nonlinear order, number of taps (DPD).

When $a = 1, b = 1, c = 2$, the optimizer selects for solutions with better ACLR than those in Table 5.10. The best solutions have a low ACLR and the optimizer selects for slightly longer filter lengths than before. This makes sense

since filter length improves ACLR while increasing the computational cost. The worst solution is one where the ACLR is just on the edge of that is acceptable. The EVM of the worst solution has a very wide margin to the EVM constraint, since that term does not contribute that much to the objective function compared to the other two. Therefore, the optimizer causes the solutions with the worst computational cost and ACLR to populate the bottom of the list.

5.5.3 Constrained optimization in six-dimensional parameter space

So far, the main focus has been put on investigating CFR clip ratio and filter length and DPD nonlinear order and memory depth. Nevertheless, the approach can be extended to other arbitrary parameters of CFR and DPD, as well as parameters of other blocks of the DFE. A possible example of other parameters to include in the optimization are:

- The number of stages in the clip-and-filter CFR block (see Section 1.4)
- The clip ratio of the hard limiter placed between the CFR and the DPD (see Section 5.4), when the block is included in the DFE chain (e.g., the block has been bypassed in the previous 4-parameters optimization).

The parameter grid used for this parameter space exploration is a large one comprised of 360 000 grid points each one corresponding to a different set of parameters. 12 238 (i.e., 3.4%) of these parameter configurations produced a solution that satisfied the constraints on the input/output signals to the PA, as defined in Section 5.5.1. The size of this simulation presented technical obstacles to visualize the results in the same way as in Section 5.5.1. Table 5.15 shows the best solutions selected by the optimizer. A value of 99 in the column for the hard limiters clip ratio signifies that the hard limiter is not present in the chain.

Cost	GFLOPS	EVM[%]	ACLR[dBc]	CR [dBc]	Fil Len	NLO	Mem	CF Stages	HL CR [dB]
2.212	37.05	2.81	-47.74	5.92	4	7	2	1	99
2.213	37.05	2.72	-47.59	6.02	4	7	2	1	99
2.217	37.05	2.90	-47.89	5.82	4	7	2	1	99
2.217	37.05	2.65	-47.42	6.12	4	7	2	1	99
2.224	37.05	2.72	-47.58	6.02	4	7	2	1	2
-	-	-	-	-	-	-	-	-	-
3.140	75.66	2.97	-47.09	7.35	8	7	4	3	0
-	-	-	-	-	-	-	-	-	-
4.578	148	2.37	-46.26	8.37	10	9	6	4	0

Table 5.15: Best, mid-range and worst values for the objective function($a = 1$, $b = 1$, $c = 1$) for a grid search over the six-dimesional parameter space: clip ratio, filter length (CFR), relative clip ratio (hard limiter), and nonlinear order, number of taps (DPD).

When the number of CFR stages was allowed to change, the optimizer heavily favoured single-stage solutions. This makes sense since the estimated computational cost is heavily dependent on number of CFR stages (see Section

3.3.2). The optimizer choses solutions with significantly lower CFR clip ratio and slightly longer CFR filters than in Section (5.5.2). The cost saved by decreasing the number of CFR stages is spent on increasing the filter length, which mitigates the ACLR and EVM effects experience when decreasing the clip ratio (more aggressive CFR). When it comes to the hard limiter, the analysis in Figure 5.29 shows that it barely affects the estimated computational cost. Therefore, a relatively large range of hard limiter clip ratio can be seen among the best solutions. Finally, the optimizer seems to privilege solution where the block switched off (slight advantage in computational cost) and where the PAPR reduction is achieved by fine-tuning the CFR and DPD blocks only.

Chapter 6

Conclusion and Areas of Future Work

6.1 Conclusion

The thesis has investigated the topic of combined parameter optimization for crest factor reduction (CFR) and digital predistortion (DPD) blocks which are commonly used in digital front ends of radio base stations. This thesis started off by giving a quick introduction to wireless communication and to the problematic of digital correction of radio impairments, such as the linearization of RF power amplifiers.

An initial review of the existing research literature covering methods for combined CFR and DPD was performed. The review has lead to identify a research gap with respect to a scarcity of methods for optimized co-design of multiple blocks of the DFE (i.e., the CFR, the hard-limiters, and the DPD blocks). The research gap has been used as starting point to design a strategy for parameter-space analysis, and to formulate a joint optimization problem which takes into account both the complexity of the digital blocks and the global performance of the DFE chain.

The above two points have been investigated as follows. A subset of the DPD and CFR parameters were selected and studied in groups of two, which also included the analysis of the effects of joint CFR and DPD parameters variation. The analysis gave a better understanding of the effects of such a parameter variation on the selected performance metrics (i.e., quality of amplified signal, signal leakage on adjacent channels, and peak envelope power presented to the PA). The results gave insights on the existence of a significant margin for operating joint parameter optimization, as CFR and DPD blocks share the same EVM and ACLR budget, and different parameters can be jointly tuned to achieve target linearization performance or complexity. An example of this is the clipping ratio of the CFR block, which directly mapped to reduced PAPR, and the nonlinear order of the DPD, which causes re-expansion of PAPR of the distorted signal while also largely driving the computational cost of the DFE chain.

In the second part of the thesis, the solution of the proposed constrained optimization problem, based on grid-search approach has been investigated. The

effects of different formulations of the proposed objective function have been also analyzed. Results have shown that, according to the specific weight factors applied to the terms of the objective function, it is possible to generate parameter sets which selectively minimize EVM (signal degradation), ACLR (adjacent channel leakage), computational cost of the DFE, or a weighted mix of the above. The thesis has also shown that the approach can be extended and include other blocks in the DFE chain, such as hard clipping stages, and supplementary parameters from the blocks (e.g., the number of CFR stages) rendering it a useful tool to guide the joint configuration of DFE blocks.

6.2 Areas of future investigation

The optimization problem studied in this thesis is relatively simplified in the sense that it is simulation-based, and it refers to an offline optimization of DPD and CFR parameters, while the best solution is simply selected among a discrete set of simulation results. Moreover, while this grid-search approach works with a limited parameter space, it is cumbersome to apply when the number of parameters, or the density of the grid in the parameter space increases.
If the dependencies between the performance metrics and the investigated parameters could be expressed algebraically, then a rigorous mixed-integer optimization problem could be formulated.

A related line of investigation is a more thorough study of the properties of the optimization problem and the investigation of alternative formulations which guarantee an optimal solution. Another possible extension of the thesis work is the inclusion of more parameters from both CFR and DPD as well as from different blocks of the DFE, e.g., hard limiters (which has been briefly analyzed as a use-case), up-samplers, and FIR filters. Two examples of those parameters are the up-sampling ratio of the signals and different points in the chain (which also greatly influences computational cost), and the length/type of FIR filters employed in the various DFE blocks. The investigation as a whole could also be expanded to include different crest factor reduction algorithms and different models and algorithms for digital predistortion, as well as more implementation-close estimations of computational costs and/or required power of the DFE.

Finally, while the current optimization has mainly targeted parameters that are used in the design of DFE and CFR blocks, the investigation of a method for joint optimization of DFE parameters at runtime is also a relevant target for future investigations, which could use the ideas and results of this work as an initial step.

Bibliography

[1] Y. Rahmatallah and S. Mohan, "Peak-to-average power ratio reduction in ofdm systems: A survey and taxonomy," *IEEE Communications Surveys and Tutorials*, vol. 15, pp. 1567–1592, Fourth 2013.

[2] ETSI, *Base Station (BS) radio transmission and reception(3GPP TS 38.104 version 16.4.0 Release 16)*.

[3] D. Morgan, Z. Ma, J. Kim, M. Zierdt, and J. Pastalan, "A generalized memory polynomial model for digital predistortion of rf power amplifiers," *IEEE Transactions on Signal Processing*, vol. 54, no. 10, pp. 3852–3860, 2006.

[4] L. Ding, G. Zhou, D. Morgan, Z. Ma, J. Kenney, J. Kim, and C. Giardina, "Memory polynomial predistorter based on the indirect learning architecture," in *Global Telecommunications Conference, 2002. GLOBECOM '02. IEEE*, vol. 1, pp. 967–971 vol.1, 2002.

[5] A. S. Tehrani, H. Cao, S. Afsardoost, T. Eriksson, M. Isaksson, and C. Fager, "A comparative analysis of the complexity/accuracy tradeoff in power amplifier behavioral models," *IEEE Transactions on Microwave Theory and Techniques*, vol. 58, no. 6, pp. 1510–1520, 2010.

[6] V. Boyd, *Convex Optimization*. Cambridge University Press, 2004.

[7] A. Farabegoli, B. Sogl, J.-E. Mueller, and R. Weigel, "A novel crest factor reduction technique using memoryless polynomials," in *2014 44th European Microwave Conference*, pp. 825–828, 2014.

[8] S. Wang, M. Roger, and C. Lelandais-Perrault, "Impacts of crest factor reduction and digital predistortion on linearity and power efficiency of power amplifiers," *IEEE Transactions on Circuits and Systems II: Express Briefs*, vol. 66, no. 3, pp. 407–411, 2019.

[9] J. Chani-Cahuana, P. N. Landin, C. Fager, and T. Eriksson, "Iterative learning control for rf power amplifier linearization," *IEEE Transactions on Microwave Theory and Techniques*, vol. 64, no. 9, pp. 2778–2789, 2016.

[10] B. Kim, J. Kim, I. Kim, and J. Cha, "The doherty power amplifier," *IEEE Microwave Magazine*, vol. 7, no. 5, pp. 42–50, 2006.

Chapter 7

Populärvetenskaplig Sammanfattning på Svenska

Gemensam CFR- och DPD-optimering för 5G sändare

Tänk om man kunde titta ut genom sitt fönster och se det osynliga som gör vårt moderna liv möjligt. Blipp!, bussbiljettens utgångsdatum är om elva dagar, grön signal. Swish!, saldo minus 29 kr, betalningen går igenom i glasskiosken. Pling!, ”-Ring mig när du kan, jag har något roligt att berätta!”.

Varje ögonblick färdas oräkneligt många signaler i ljusets hastighet mitt framför näsan på oss utan att vi märker något. Allt som skedde utanför fönstret möjligjordes genom att elektromagnetiska vågor färdades mellan mobiltelefoner och sändare i master. När en mast sänder ut en signal måste den förstärkas för att den ska nå mottagaren. Problemet är att förstärkare ofta beter sig oberäkneligt och förvränger signalen. Ju högre spänning förstärkarens insignal har desto värre blir dessa förvrängningar. Om man har otur försämras signalens kvalité till den grad att datan den bär på blir oläslig. Bruset den orsakar kan även störa signaler i grannkanaler, därför måste utsignalen uppfylla kvalitétskrav som bestäms av myndigheter. Man skulle kunna undvika detta genom att mata förstärkaren med en svagare signal, men då försämras förstärkarens verkningsgrad och räckvidd väsentligt. För att kringå denna avvägning mellan signalkvalité och verkningsgrad kan man manipulera signalen på ett sätt som kompenserar för förstärkarens brister. Det finns många metoder att göra detta på och detta examensarbete har undersökt kombinerad digital förförvrängning och klippfiltrering. Klippfiltrering sätter ett tröskelvärde och klipper bort den delen av insignalen vars spänning överskrider det. Dessa spänningstoppar som klipptes bort var den delen av signalen som orsakade mest förvrängnining och brus i förstärkaren. Klippandet i sig orsakar också brus men denna bruskällan undgås genom att man filtrerar den avklippta delen av signalen och subtraherar den från den ursprungliga. Ju lägre tröskelvärde, desto högre spänning kan man mata förstärkaren med, men är det för lågt så kan signalen förändras så mycket att dess data förstörs. Digital förförvrängning gör en modell av förstärkarens oberäkneliga beteende och använder den för att förvränga insignalen på ett sådant sätt att den får en linjär, förutsägbar förstärkning när den skickas ut i nätet. Sambandet mellan parametrarna i dessa metoder och olika mått på signalkvalité och brus är komplext vilket gör det svårt att kalibrera dem. I denna undersökning utforskades olika digital förförvrängnings- och klippfiltrerings parametrar systematiskt genom simuleringar på en virituell förstärkare. Ett mångsidigt optimeringsverktyg skapades för att kalibrera parametrarna till dess optimala värde. Optimeringsverktyget rangordnar lösningar baserat på dess signalkvalité och brusutsläpp samt hur mycket datorkraft det kostar att implementera dem.

-Gustav Olsson